

REVIEW

[View Article Online](#)
[View Journal](#) | [View Issue](#)Cite this: *J. Mater. Chem. A*, 2022, 10, 1682Synthetic solid oxide sorbents for CO₂ capture: state-of-the art and future perspectivesRibooga Chang, ^{†a} Xianyue Wu, ^{†bc} Ocean Cheung ^{*a} and Wen Liu ^{*b}

Carbon capture is an important and effective approach to control the emission of CO₂ from point sources such as fossil fuel power plants, industrial furnaces and cement plants into the atmosphere. For an efficient CO₂ capture operation, many aspects of the CO₂ capture steps need to be carefully considered. Currently the most mature CO₂ capture technology is liquid amine scrubbing. Alternatively, solid sorbents can be used to effectively capture CO₂ while alleviating the disadvantages associated with liquid amine sorbents. In this review, we critically assess solid metal oxide CO₂ sorbents, especially oxides of group 1 (Li, Na and K) and group 2 (Mg, Ca, Sr and Ba) metals, for capturing CO₂ at moderate to high temperatures. In particular, we focus on the recent advances in developing synthetic metal oxide sorbents, and the correlation between the design, synthetic approaches and their cyclic CO₂ capture performance, which are characterised by CO₂ uptake capacity, rate of carbonation and cyclic stability. The state-of-the-art, challenges, opportunities and future research directions for these metal oxide sorbents are discussed. By devoting more research effort to address the issues identified, there can be great potential to utilise Group 1 and 2 metal oxides as cost-effective, highly efficient sorbents for CO₂ capture in a variety of carbon capture applications.

Received 7th September 2021
Accepted 19th December 2021

DOI: 10.1039/d1ta07697c

rsc.li/materials-a

^aDepartment of Materials Science and Engineering, Nanotechnology and Functional Materials, Uppsala University, SE75121, Sweden. E-mail: ocean.cheung@angstrom.uu.se

^bSchool of Chemical and Biomedical Engineering, Nanyang Technological University, 62 Nanyang Drive, 637459, Singapore. E-mail: wenliu@ntu.edu.sg

^cInterdisciplinary Graduate Programme, Nanyang Environmental & Water Research Institute, 1 Cleantech Loop, 637141, Singapore

[†] These authors contributed equally to this work.



Ribooga Chang is a PhD student at the Department of Materials Science and Engineering at Uppsala University, Sweden. Ribooga holds a master's degree from Gwangju Institute of Science and Technology (GIST), Korea. Her PhD work has been focused on the development of high-temperature sorbents and porous materials for a number of applications e.g. gas separation, water treatment, and drug delivery.



Xianyue Wu is a doctoral student in Chemical Engineering at the School of Chemical and Biomedical Engineering, Nanyang Technological University. Xianyue is also enrolled on an Interdisciplinary Graduate Programme in collaboration with Nanyang Environment & Water Research Institute (NEWRI), Residues, Resource and Reclamation Centre (R3C). She has a Bachelor of Engineering (Chemical and Biomolecular Engineering) with Honours (Highest Distinction) degree from Nanyang Technological University, Singapore. Her research interests include catalyst and process development in thermal catalysis of carbon monoxide and carbon dioxide. She is currently focusing on work regarding nickel-based dual function material for CO₂ capture and conversion.



1 Introduction

1.1 Background

Global warming is one of the major challenges of the present century.¹ The high concentration of CO₂ in the atmosphere due to human activity is indisputably the main cause of global warming. In particular, the combustion of fossil fuels for electricity generation, transportation, oil refining, cement production and metallurgy results in the release of CO₂ into the atmosphere at a rate that is far beyond what the ecosystem can take up.² Therefore, decarbonisation technologies have been one of the focal points of research in science and engineering. In a sustainable and low-carbon future, renewable energies will eventually replace fossil fuels. In the meantime, the carbon capture, storage and utilisation scheme (CCSU) will play an important role as a transitional solution to provide low-emission hydrogen, electricity and CO₂-derived products from fossil fuel feedstocks. After renewable energies have completely decarbonised the energy sector, CCSU will continue to be relevant to industrial processes such as steelmaking and cement production.³

The first step in CCSU is the capture of CO₂ from point sources of emissions or, in the case of direct air capture (DAC), from the atmosphere. When capturing from the combustion of fossil fuels, three main strategies exist: pre-combustion, post-combustion and oxy-fuel combustion. Pre-combustion capture involves extracting CO₂ from syngas during hydrogen production (by gasification, reforming and downstream purification processes), followed by the combustion of the “blue hydrogen” produced. Post-combustion capture is an end-of-pipe strategy that extracts CO₂ from the combustion flue gases. Oxy-fuel combustion proceeds by burning carbonaceous fuels in the absence of nitrogen. The flue gas of oxy-fuel combustion, after the removal of water, NO_x, SO_x and any residue N₂, can be considered captured. The interested reader is referred to Stanger *et al.*⁴ for detailed discussions of various carbon capture strategies.

Regardless of the strategy, CO₂ capture requires gas separation, which can be achieved by various technologies including chemical scrubbing, physical adsorption (physisorption), cryogenic distillation, membrane separation, *etc.* Currently, chemical scrubbing using amine solutions is the most mature carbon capture technology, which can be deployed at commercially viable scales.⁵ However, CO₂ capture by amine scrubbing is energy intensive (typically 4–6 MJ kg^{−1} CO₂ captured by monoethanolamine).⁶ In addition, liquid amine solutions are expensive to produce, corrosive, and suffers from thermal and oxidative degradation during regeneration (although some priority amine formulations claim superior cyclic stability).⁷

Physical sorption processes utilise sorbents in either liquid form (*e.g.* selexol) or solid form (*e.g.* zeolites and metal-organic framework) and do not require high operating temperatures.^{8,9} Instead, the regeneration of physical sorbents requires strong vacuum and/or gentle heating, which are associated with unrecoverable energy penalty. Physisorbents such as zeolites, zeotypes, metal-organic frameworks (MOFs) tend to perform best at ambient temperatures with respect to CO₂ uptake capacity: zeolites and zeotype typically have high CO₂ uptake at low pressures in the range of approximate 4–25 wt% up to 1 bar at ambient temperatures.¹⁰ MOFs perform comparably better at high pressures, CO₂ uptake at ambient temperatures of well over 100 wt% have been reported close to the saturation pressure of CO₂ (*e.g.* NU-1000).^{11,12} It is important to note that these physisorbents do not have high CO₂ uptake at high temperatures (*i.e.* the temperature of combustion flue gas) and therefore, the possible use of physisorbents in CO₂ will require cooling of the flue gas. In addition, most physical sorption technologies are not specifically selective towards CO₂ and must operate under dry conditions to avoid water competing for adsorption sites. This need to de-humidify the gas feed adds extra costs. Although hydrophobic sorbents have been developed to tackle the problem associated with selectivity towards water,^{13,14} there remains a need to reduce the production cost of these complex synthetic sorbents. As an alternative, cryogenic separation technologies



Ocean Cheung is an assistant professor at the Division of Nanotechnology and Functional Materials at Uppsala University, Sweden. He holds a Master of Chemistry (MChem) degree from the University of Warwick, UK and a PhD in Materials Chemistry from Stockholm University, Sweden. His research is focused on the development of functional porous materials for environmental and bio-applications.

Focused application areas within Dr Cheung's research include gas/vapour adsorption/separation, catalysis water treatment, and controlled drug delivery.



Wen Liu completed his training as a chemical engineer at the University of Cambridge. He is currently an Assistant Professor at the School of Chemical and Biomedical Engineering, Nanyang Technological University. Dr Liu's research focuses on studying carbon capture and utilisation (CCU) processes, from understanding the atomic scale reaction mechanisms, to designing new CCU strategies

using process intensification strategies. He has a special interest in using hypothesis-driven methods to develop high performance oxide materials for carbon capture, oxygen transport, thermochemical water splitting and heterogeneous catalysis.



exploit the difference in the boiling points of the gas molecules, such that CO₂ can be extracted from the process gas mixtures *via* distillation or anti-sublimation.¹⁵ Therefore, cryogenic separation is capable of producing CO₂ of very high purity that can be readily transported and utilised without further processing. However, the supply of cryogenic chill is often costly, both in terms of capital expenditure (CAPEX) and operational costs (OPEX), unless a low-cost cold energy source (*e.g.* the latent heat of the vaporisation of liquified nature gas) is available.¹⁶

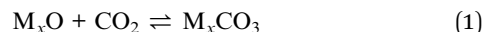
Membrane technology offers process simplicity and scalability for extracting CO₂ from gas mixtures.¹⁷ Unfortunately, the requirement for high pressure gradients across the membranes and the low durability of the membrane materials present notable technical challenges to the large-scale deployment of membrane-based for CO₂ capture technologies.¹⁸

In order to address the practical issues (*e.g.* thermal degradation and corrosiveness) associated with liquid amine scrubbing, the use of solid sorbents, such as solid amines and alkali metal oxides, has been proposed. In the latter case, the solid oxide sorbents occupy a large compositional space with versatile chemical formulations that can be tailored for a variety of CO₂ capture applications.¹⁹ For example, the temperatures at which the sorbents take up and release CO₂ can be tuned by design. Different types of sorbents (*e.g.* physisorbents, liquid absorbents and high temperature solid sorbents) take up CO₂ *via* different mechanisms and have different operational conditions, it is therefore, not always possible to compare the different types of sorbents directly. Here, we review the recent developments of solid oxide sorbents, with a focus on synthetic strategies towards improved CO₂ capture performance.

1.2 Reversible CO₂ uptake by metal oxide sorbents

Metal oxides capable of chemically taking up CO₂ typically contain alkali metals and, or alkaline earth metals. The

reversible capture of CO₂ by the metal oxide sorbents can be generalized by:



where $x = 1$ and 2 for alkaline earth metals and alkaline metals, respectively. The forward reaction involves carbonating the sorbent in flue gases with typical CO₂ mole fractions in the range of 3–20%. The carbonation takes place in the carbonator exothermically at a low temperature, at which the equilibrium CO₂ partial pressure is below 0.001 bar, such that almost all the CO₂ in the gas stream can be cleaned up by the sorbent. The reverse reaction (*i.e.* sorbent regeneration) involves decomposing the carbonate produced in virtually pure CO₂, such that the gaseous product is also a stream of pure CO₂, which can be further purified and compressed for storage and, or utilisation. The regeneration takes place endothermically at a high temperature, at which the equilibrium CO₂ partial pressure of the reaction system exceeds 1 bar, so all of the carbonated sorbent would irreversibly decompose. Plots of the equilibrium partial pressures of CO₂ for the carbonation of the binary oxides of alkali metals and alkaline earth metals are shown in Fig. 1a. Note that Fig. 1a excludes elements that are either deemed too expensive (*viz.* Rb₂O and CsO) or having considerable radioactivity (*viz.* Fr₂O and RaO). Based on the equilibrium temperatures for reversible CO₂ capture and regeneration, we define three types of solid oxide sorbents: (i) CaO, which reversibly takes up CO₂ at high temperatures, (ii) MgO, which reversibly takes up CO₂ at near-ambient temperatures, and (iii) all other oxides (Li₂O, Na₂O, K₂O, SrO and BaO), which are very strong bases whose carbonates require impractically high temperatures (*e.g.* above the melting point of the carbonates) to decompose. The ease to decompose the carbonates (as depicted in Fig. 1a) correlates well to the optical basicity of the binary



Fig. 1 (a) Equilibrium curves of partial pressures of CO₂ for the carbonation of the binary oxides of alkali metal/alkaline earth metal as functions of temperature. The red shaded area indicates CO₂ partial pressures that are practically achievable in a continuous CO₂ capture system. The discontinuities of the equilibrium curves changing from solid lines to dashed represents the melting point of the corresponding carbonates. (b) Schematic illustration of post-combustion CO₂ capture by solid sorbents in interconnected fluidised beds.



Table 1 Optical basicity of oxides based sorbents^{23,24}

| Cation | Oxide | Basicity |
|------------------|-------------------|----------|
| Mg ²⁺ | MgO | 0.78 |
| Ca ²⁺ | CaO | 1.0 |
| Li ⁺ | Li ₂ O | 1.0 |
| Sr ²⁺ | SrO | 1.1 |
| Ba ²⁺ | BaO | 1.15 |
| Na ⁺ | Na ₂ O | 1.15 |
| K ⁺ | K ₂ O | 1.4 |

metal oxides, as shown in Table 1, *i.e.* the carbonates derived from oxides with high optical basicity are generally hard to decompose during regeneration. Therefore, the basicity of type (iii) oxides are often chemically modified to enable reversible CO₂ uptake under practically accessible conditions.

As there is a temperature gap between the carbonation and the calcination steps, continuous CO₂ capture typically requires circulating the sorbents between two reactors, *viz.* a carbonator and a calciner. A common reactor configuration to achieve the swings between carbonation and regeneration is a set of interconnected fluidised beds, as depicted in Fig. 1b.^{20–22}

Microscopically, the solid oxide sorbent particles undergo significant morphological changes as they cyclically take up and release CO₂. Although the carbonation of different types of sorbents follows different reaction mechanisms, there are some commonalities. During CO₂ capture, the sorbent typically develops a layer of carbonate, restricting the access of CO₂ to the unreacted oxides, thus reducing the overall rates of CO₂ uptake. In addition, the carbonates formed generally have low melting points, causing the sorbents to sinter, thereby hindering their performance in subsequent capture cycles. Because of these limitations, there are considerable gaps between the sorbents' stoichiometric CO₂ uptake capacities and those practically accessible after multiple carbon capture cycles. To improve the overall efficiency and effectiveness of the oxide-based CO₂ capture processes, a significant amount of research is required to understand the sorbent behaviour and subsequently to rationally design high performance sorbents, often by optimising the synthesis approach. In general, an ideal solid oxide sorbent should (i) be able to undergo reversible carbonation at temperatures that are closely matching the temperatures of the upstream/downstream processes, (ii) have fast uptake and release kinetics, (iii) exhibit stable performance over large number of CO₂ capture cycles, (iv) have sufficient physical hardness to survive prolonged attrition in circulating fluidised beds and (v) can be produced in large quantities with relatively simple methods and low costs.

1.3 Objective and review outline

Over the past decades, there have been large number of studies that develop and investigate solid oxide CO₂ sorbents, with focuses on both the process and materials aspects. The interested reader is referred to past reviews which provide broad overviews of CO₂ capture technologies employing solid sorbents,²⁵ and in particular metal oxide-based solid sorbents.²⁶

It is worth noting that the studies addressing the materials challenge ubiquitously point towards the need to develop high-performance synthetic sorbents. Despite the abundant reports of synthetic sorbents showing improvements over natural sorbents such as limestone, the relationships between the sorbents' compositions, synthesis methods, structures and CO₂ capture behaviour are still not fully understood. Therefore, given the rapid development in characterisation techniques and synthesis methods, we see the need for a critical assessment of the literature focusing the recent advances in synthetic strategies for preparing high performance metal oxide based CO₂ sorbents with the following specific objectives:

- Review the state-of-the-art understanding of the behaviour of the oxide sorbents over CO₂ capture cycles.
- Review different synthetic approaches for preparing high performance oxide sorbents.
- Identify knowledge gaps in understanding the behaviour of synthetic sorbents under realistic CO₂ capture conditions.
- Highlight emerging approaches for improving the performance of synthetic sorbents.
- Promote the need for standards for evaluating the performance of newly developed CO₂ sorbents.

2 CaO based sorbents

CaO based sorbents are the most commonly discussed due to their high CO₂ uptake capacity, fast carbonation and regeneration rates, high earth-abundance and low cost. In Table 2 we summarise the CO₂ uptake properties of a number of recently reported CaO based CO₂ sorbents. The reversible reaction between CaO and CO₂ is also known as calcium looping or calcium carbonate looping:



The forward reaction typically takes place around 650 °C, whereas regeneration takes place in 1 bar CO₂ at >900 °C.⁴ The CaO sorbents can be applied to both pre- and post-combustion CO₂ capture at power stations, as well as CO₂ capture from industrial processes such as cement production.^{27,28} In the case of pre-combustion capture,²⁹ CaO facilitates the sorbent-enhanced water gas shift to produce highly concentrated H₂:³⁰



In addition, CaO based sorbents can be used for capturing CO₂ produced by cement plants.³¹ In fact, CaO based capture process can be efficiently integrated into the cement production process,³² requiring only minor modifications to the existing equipment and process, whilst reducing the fuel consumption and CO₂ emissions by ~75% and ~85%, respectively.³³ Because of the relative ease to prepare CaO based sorbents at large batches, the integration of CaO based carbon capture has been demonstrated at pilot scales (to up 1.9 MWth) by various research groups.^{34,35} Freshly prepared CaO sorbents, without any further modification, could easily take up CO₂ close to the



Table 2 Various reaction conditions and capacities of CaO based sorbents^a

| Sorbent | Conditions | | | | | Capacity | | | | | | | |
|---|---------------------|--|---|---------------|------------------------------|------------------------------|------------------------|------------------------|---------------------|---------------------------------------|------------------------------|------------------------------|------|
| | Name of the sorbent | Base (B) | Support (S) | Fraction of S | Carbonation temperature [°C] | Calcination temperature [°C] | Carbonation time [min] | Calcination time [min] | CO ₂ [%] | BET [m ² g ⁻¹] | CO ₂ uptake [wt%] | Cycle capacity [loss%/cycle] | Ref. |
| S20-4x | | Ca(NO ₃) ₂ ·4H ₂ O | Zr(NO ₃) ₂ ·6H ₂ O | 0.1 | e | 675 | 850 | 20 | 10 | 20 | 12 | 41.8 53.3 0.8/20 | 53 |
| S20-6x | | Ca(NO ₃) ₂ ·4H ₂ O | Zr(NO ₃) ₂ ·6H ₂ O | 0.1 | e | 675 | 850 | 20 | 10 | 20 | 20 | 49.7 63.4 7.3/20 | 53 |
| S20-8x | | Ca(NO ₃) ₂ ·4H ₂ O | Zr(NO ₃) ₂ ·6H ₂ O | 0.1 | g | 675 | 850 | 20 | 10 | 20 | 23 | 48.9 62.2 5.7/50 | 53 |
| CL-CE-75 | | Calcium L-lactate hydrate | CaO·Al ₂ O ₃ cement | 0.25 | f | 650 | 900 | 30 | 10 | 15 | — | 36 45.9 —/70 | 74 |
| CC-AN-80 | | | | | | | | | | | | | |
| Ca ₃ (C ₆ H ₅ O ₇) ₂ ·4H ₂ O | | Al(NO ₃) ₃ | 0.2 | b | 800 | 30 | 10 | 15 | 10 | 59 | 75.2 14/28 75 | | |
| CaO-SBA15 | | Ca(CH ₃ COO) ₂ | SBA | 0.5 | b | 700 | 910 | 60 | 30 | 100 | 155 | 43.1 55 20/40 | 76 |
| CaO-CC | | CaCO ₃ | — | — | — | 650 | 120 | 950 | 30 | 15 | 1 | 71.2 90.7 23.75/11 | 77 |
| CaO-ES | | CaCO ₃ | MgCO ₃ | — | — | 650 | 120 | 950 | 30 | 15 | 1 | 61.8 78.8 20.41/11 | 77 |
| CaO-P | | CaCl ₂ | — | — | c | 650 | 120 | 950 | 30 | 15 | 5 | 48.6 61.9 2.97/11 | 77 |
| Ca-Al-CO ₃ | | CaO | Al ₂ O ₃ | 0.5 | c | 600 | 700 | 45 | 20 | 50 | — | 55.7 71 —/10 | 66 |
| Ca-Al-CO ₃ | | CaO | Al ₂ O ₃ | 0.5 | c | 600 | 700 | 25 | 20 | 50 | — | 56.7 72.3 —/30 | 66 |
| Ca ₁ Ni _{0.1} | | Ca(NO ₃) ₂ ·4H ₂ O | Ni(NO ₃) ₂ ·6H ₂ O | 0.1 | d | 650 | 650 | 25 | 3 | 15 | 13 | 66.0 84.1 —/20 | 55 |
| Ca ₁ Ni _{0.1} Ce _{0.033} | | Ca(NO ₃) ₂ ·4H ₂ O | Ce(NO ₃) ₂ ·6H ₂ O | 0.033 | d | 650 | 650 | 25 | 3 | 15 | 21 | 62.1 79.1 —/20 | 55 |
| CNAN-SG | | Ca(NO ₃) | Al(NO ₃) ₃ ·9H ₂ O | 0.3 | d | 650 | 900 | 5 | 5 | 15 | 13 | 27.5 35 28/21 | 65 |
| CAAN-SG | | Ca(CH ₃ COO) ₂ | Al(NO ₃) ₃ ·9H ₂ O | 0.3 | d | 650 | 900 | 5 | 5 | 15 | 12 | 13.6 17.3 40/21 | 65 |
| CaO-GS 2 mM | | CaO | Gemini surfactant | 0.0008 | f | 600 | 850 | — | 30 | 15 | 16 | 29.0 37 — | 72 |
| CaO-SDS 20 mM | | CaO | Sodium dodecyl sulfate | 0.008 | f | 600 | 850 | — | 30 | 15 | 9 | 27.0 34.4 — | 72 |
| CaO-(s-s) | | CaO | ZrO ₂ | 0.03 | e | 650 | 780 | 120 | 60 | Pure | — | 57.7 73.5 — | 58 |
| CaO-(c-sg) | | CaO | ZrO ₂ | 0.03 | d | 650 | 780 | 120 | 60 | Pure | — | 77.5 98.7 — | 58 |
| CaO/CaZrO ₃ | | Ca(NO ₃) ₂ ·4H ₂ O | ZrO(NO ₃) ₂ ·xH ₂ O | 0.14 | d | 650 | 850 | 30 | 5 | 15 | — | ~48.0 61.1 7/50 | 68 |
| CaO-ZrO ₂ -SG | | CaO | ZrO ₂ | 0.1 | d | 200 | 900 | — | — | — | 25 | 65.0 82.8 —/20 | 59 |
| CaO-ZrO ₂ -IM | | CaO | ZrO ₂ | 0.1 | b | 200 | 900 | — | — | — | 19 | 64.0 81.6 6.25/14–20 | 59 |
| Ca-hyd_95:5_2 h | | Ca(OH) ₂ | ZrO ₂ | 0.05 | d | 800 | 800 | 5 | 15 | 50 | 12 | 51.0 65 39.22/90 | 78 |
| Ca-hyd_95:10_2 h | | Ca(OH) ₂ | ZrO ₂ | 0.1 | d | 750 | 750 | 20 | 10 | 40 | 11 | 52.0 66.3 5.77/10 | 78 |
| C74D26 | | Carbide | Dolomite | 0.35 | a | 700 | 850 | 20 | 10 | 15 | 14 | 54.0 68.9 —/10 | 79 |
| Mg/Ca-0.2 | | Ca(CH ₃ COO) ₂ | Mg(NO ₃) ₂ | 11 | d | 700 | 700 | 30 | 30 | Pure | — | 59.2 75.4 4.7/7 | 80 |
| Ca/Al-2.5-1% | | CaO | Al ₂ O ₃ | 0.4 | c | 600 | 700 | 45 | 20 | 100 | 6 | 59.1 75.3 5.9/220 | 48 |
| Ca-CNT | | CaO nanotube | — | — | — | 650 | 850 | 30 | 10 | 15 | 12 | 58.0 73.9 34.48/15 | 81 |

^a (a) Combustion, (b) impregnation, (c) precipitation, (d) sol-gel, (e) solid-state, (f) wet-mixing, (g) solution-combustion.

stoichiometric capacity of 78 wt% (based on the mass of the fully calcined CaO)^{36,37} however, the performance of unmodified CaO sorbents will rapidly deteriorate over uptake–regeneration cycles as a result of sintering,^{38,39} as the surface area and accessible pore volumes of the sorbents rapidly diminish. In continuous operation, the deactivated sorbents act as inert materials, which imposes significant energy penalty as they participate in the temperature swing cycles without capturing CO₂. The deactivation mechanism during calcium looping cycles has been extensively studied.^{32,40–42} The biggest challenge of using CaO sorbents is to develop solutions that address their poor cyclic stability. The two general strategies to improve the performance of calcium looping systems are (i) optimising operating conditions and (ii) prepare high performance synthetic sorbents, as discussed in the following sections.

2.1 Optimising operating conditions

The performance of the CaO based sorbents depends on the operating conditions. Accordingly, researchers have exploited such dependence to delay or mitigate sorbent deactivation over calcium looping cycles. For example, the presence of steam in the calcium looping reactors is found to influence both reaction rates and mass transfer^{43,44} specifically, steam is known to enhance the rate of calcination.^{45,46} In addition, experimental observations suggest that operation in the presence of steam increases the porosity of the sorbents, and subsequently improve their CO₂ capture performance in terms of both reaction kinetics and cyclic stability.^{47,48}

The issue of sorbent deactivation can also be circumvented by reactivating the spent sorbents. The recent study by Sun *et al.*⁴⁹ provided insights into the effects of different reactivation methods on the cyclic performance of CaO/MgO (CaO : MgO mass ratio = 75 : 25) sorbents, obtained using calcium acetate monohydrate and magnesium acetate tetrahydrate as precursors. Sun *et al.*⁴⁹ tested different sorbent reactivation methods: (i) hydration, (ii) hydration/impregnation and (iii) acidification. Good cyclic stability was observed when the sorbent was reactivated by hydration or hydration/impregnation, rendering CO₂ uptake of 39 and 41.4 wt% (49.7 and 52.8 mol%) after 40 cycles, respectively. In both cases, the CO₂ uptake increase with the number of cycles due to “self-activation”. Self-reactivation,



Fig. 2 The pore skeleton model for CO₂ and ion diffusion. Illustrated according to the finding presented in ref. 51.



Fig. 3 Scanning electron micrograph of CaO stabilised with both MgO and Al₂O₃ (left) as-synthesised and (right) after 23 cycles of carbonation/calcination.⁵⁶

sometimes referred to as “deep carbonation”, is a phenomenon that can be explained using the pore skeleton model by Manovic and Anthony,⁵⁰ as depicted in Fig. 2. An inward hard skeleton is formed during calcination. However, the hard skeleton hampers the ion diffusion through the product layer of CaCO₃, impeding the rate of carbonation during the initial cyclic operation. Over the carbonation–regeneration cycles, the soft skeleton is gradually activated and contributes to an increase rate of carbonation.⁵⁰

Sorbent reactivation by acidification is relevant for removing the irreversibly formed CaSO₄ due to the presence of SO₂ in the flue gas. For a CaO : MgO sorbent, reactivation by acidification resulted in a CO₂ uptake of 23.3 wt% (29.7 mol%) after 40 cycles. Thus, acidification as a reactivation method needs further development to overcome the high cost and the potential release of toxic substances.⁴⁹

2.2 Synthetic CaO based sorbents stabilised by inert supports

In addition to employing reactivation steps, the cyclic performance of CaO sorbents can be fundamentally improved by mixing CaO with inert refractory materials (*e.g.* Al₂O₃, ZrO₂,

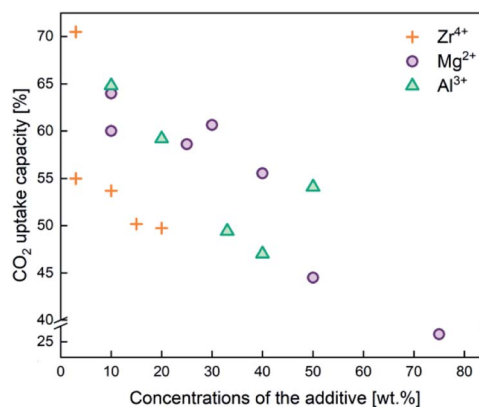


Fig. 4 CO₂ capture capacity of CaO based sorbents stabilised by the three different typical sintering-resistant, oxidic additives containing Zr⁴⁺, Al³⁺, and Mg²⁺. The effect of these additives on the cyclic stability of CaO sorbents is summarised in Table 2.



MgO and their derivatives) to render additional sintering resistance and physical hardness. A number of studies have reported CaO based sorbents supported on varying amounts of refractory materials. The resulting CO₂ uptake capacity also varied, partly due to the differences in the overall compositions, as shown in Fig. 4. The stabilising effects of adding different types and amounts of thermally stabilising cations, referencing notable recent works, are summarised in Table 2 and discussed below.

Soleimanisilim *et al.*⁵² used CaCl₂·2H₂O and a small amount of ZrO(NO₃)₂·6H₂O as precursors to prepare a stabilised CaO sorbent containing 10 wt% CaZrO₃ perovskite by the solution combustion method. The resulting CaO sorbent showed a high CO₂ uptake of ~53.3 wt% (68.2 mol%) in the first cycle and ~42.7 wt% (54.41 mol%) after 31 cycles. The stabilising effect of CaZrO₃ was also reported by Hashemi *et al.*⁵³ who found 20 wt% CaZrO₃ to be optimal for maintaining cyclic stability (46.2 wt% (58.87 mol%) after 20 cycles). To maximise cyclic stability and CO₂ capture performance, the type of stabiliser and the amount of stabiliser were optimized in the relevant studies.^{43,44} Specifically, Guo *et al.*³⁹ showed that the Ca : Al ratio of Ca–Al mixed oxides (Ca²⁺/Al³⁺ = 2, 2.5, 3, 3.5, 4) synthesised by coprecipitation affected the CO₂ uptake capacity. The Ca : Al ratio of 2.5 gave the highest CO₂ uptake capacity of around 47 wt% (60 mol%) after 3 cycles. The high CO₂ capacity and reasonable cyclic performance was attributed to the large pore size and the small particle size. Compared to the morphological properties, the amount of Ca₁₂Al₁₄O₃₃ present was also found to be a crucial factor in determining the sorbent's CO₂ capture capacity.^{48,52,54} Sun *et al.*⁵⁵ revealed that CeO₂ can be used as an effective physical barrier to prevent the sintering of CaO. Similarly, Vall *et al.*⁵⁶ employed MgO and Al₂O₃ to stabilise a synthetic CaO sorbent, obtained by calcining highly porous amorphous calcium carbonate (HPACC–BET surface area of over 450 m² g^{−1}). Whilst MgO alone can effectively stabilise the CaO sorbent, the sorbent synergistically stabilised by both MgO and Al₂O₃ yielded even higher stability, showing only a 2.8% decrease in the CO₂ uptake capacity after 23 cycles (1st cycle 54.2 wt%, 69.1 mol%). Scanning electron micrographs (SEM) (Fig. 3) of the CaO stabilised with both MgO and Al₂O₃ confirmed the effective hinderance of sintering after 23 cycles.

2.2.1 Preparing supported sorbents by sol–gel method. The effective mixing between CaO and thermal stabilisers (*i.e.* support materials) is critical to enhancing the cyclic CO₂ capture performance. Conventional preparation methods, such as mechanical mixing, impregnation and co-precipitation may not provide sufficient dispersion of the thermal stabilisers within the sorbent matrix. To this end, sol–gel method has been explored as an alternative strategy to prepare supported CaO sorbents.⁵⁷ In general, sol–gel methods can induce and control the chemical interaction between the inert supports and CaO, whilst allowing the facile control of particle size and surface area. Yoon *et al.*,⁵⁸ Sultana *et al.*⁵⁹ and Gao *et al.*⁶⁰ all showed that CaO based sorbents prepared by sol–gel synthesis result in increased specific surface areas and pore volumes. The increased porosity can come from reduced particle size, leading to shortened CO₂ diffusion paths and consequently accelerated



Fig. 5 CO₂ capture capacity of nano-CaO by sol–gel and wet impregnation methods. Reprinted with permission from ref. 59. Copyright 2021 American Chemical Society.

rate of CO₂ capture. For example, Zr-modified CaO prepared by Yoon *et al.*⁵⁸ had small particle sizes of ≤ 2 μm, high CO₂ uptake of 73.2 wt% (93.3 mol%) (compared to 54 wt% (69 mol%) of the sorbent prepared by physical mixing). In addition the CO₂ uptake capacity sustained at ~70.5 wt% (89.8 mol%) over 10 cycles.⁵⁸ Sultana *et al.*⁵⁹ prepared nano-CaO coated with ZrO₂ by sol–gel, wet impregnation, and hydrolysis methods. They found that sol–gel synthesis gave the most stable CaZrO₃ protective layer on the surface of the nano-CaO, with excellent CO₂ uptake of 65 wt% (83 mol%) after 20 cycles, as shown in Fig. 5.⁵⁹ Similarly, Gao *et al.*⁶⁰ synthesised CaO supported on charcoal by physical mixing, sol–gel, and wet impregnation and found that the CaO supported on charcoal by sol–gel method showed a high CO₂ capture capacity of 66.5 wt% (84.7 mol%).⁶⁰ In both studies, the sol–gel methods produced sorbents with the higher pore volumes, surface areas, CO₂ uptake and cyclic stability than sorbents prepared by other methods.

2.2.2 Core-shell structured sorbents. One special type of stabilised CaO based sorbents is core-shell structured sorbents, where the stabilising oxides form shells encapsulating the CaO cores. In effect, the inert shells form continuous physical barriers, preventing the cores from fusing into each other. Han *et al.*⁶¹ synthesised the CaO@Al₂O₃ core-shell structure sorbent and observed 41 wt% (52 mol%) of CO₂ uptake after 20 cycle with Al₂O₃ shell thicknesses of between 4 to 8 nm. The covered cores (CaO) have resisted sintering over CO₂ capture cycles.⁶¹ The thickness of the shell can be one of the factors determining the overall CO₂ capture performance. Armutlulu *et al.*⁶² prepared CaO@Al₂O₃ core-shell sorbents, with three different shell thicknesses. The thickness around 2.75 nm reported relatively good stability and CO₂ uptake capacity of ~55 wt% (70 mol%) after 30 cycles, whereas thicker Al₂O₃ layers lead to lower initial CO₂ uptake.⁶² In addition to the CaO@Al₂O₃ design, Peng *et al.*⁶³ added TiO₂ as a secondary stabiliser. The resulting CaO@TiO₂-Al₂O₃ showed high stability and CO₂



uptake of 46 wt% (59 mol%) after 104 cycles.⁶³ Using a 2.7 nm Al_2O_3 coating on CaO nanoparticles, Kurlov *et al.*⁵⁴ demonstrated a 140% improvement in CO_2 uptake over a limestone reference and excellent cyclic stability (41 wt% (52 mol%) uptake after 10 cycles). They found the addition of the Al_2O_3 layers induced the formation of inert $\text{Ca}_{12}\text{Al}_{14}\text{O}_{33}$ and $\text{Ca}_3\text{Al}_2\text{O}_6$ on the surface of CaO nanoparticles, produced by the calcination of calcite obtained by sacrificial template synthesis, with an average particle size of 350 nm and a BET surface area of $16 \text{ m}^2 \text{ g}^{-1}$. Consequently, the shell layer consisting of $\text{Ca}_{12}\text{Al}_{14}\text{O}_{33}$ and $\text{Ca}_3\text{Al}_2\text{O}_6$ acts as an effective thermal stabiliser.⁵⁴

2.2.3 Effect of synthesis parameters. It is well established that the CO_2 uptake performance, including kinetics and cyclic stability, are functions of the sorbents' starting structures, which are in turn determined by the synthesis parameters used during sorbent preparation. For early literature on the synthesis of CaO based sorbents, we refer the reader to the reviews by Liu *et al.*⁶⁴ and Kierzkowska *et al.*²⁹ Here, we focus on recent studies (last ~5 years) investigating the effects of key synthesis parameters, as discussed in the following.

Precursors. Although the exact roles and effects of the various chemical precursors may differ, they are nonetheless critical to the performance of the synthesised sorbents. Azimi *et al.*⁶⁵ demonstrated that different combinations of Ca and Al precursors yield sorbents with noticeably different particle sizes, surface areas and morphologies. For instance, for the sol-gel synthesis of a CaO based sorbent, highly soluble nitrate precursors such as calcium nitrate (CN) and aluminium nitrate (AN) form inert phases such as $\text{Ca}_{12}\text{Al}_{14}\text{O}_{33}$ and $\text{Ca}_9\text{Al}_6\text{O}_{18}$ more easily than the nitrate-free precursors. The insoluble precursors such as nano-structured alumina (nA) formed a more compact structure than the ones prepared from aluminium nitrate (AN), which yielded a "fluffy structure" with a surface area of $13 \text{ m}^2 \text{ g}^{-1}$ and a mean particle size ~16.9 nm. Overall, the Al-supported CaO sorbent synthesised with soluble nitrate precursors showed the highest CO_2 uptake (91.7 wt% (117 mol%), with 28 wt% loss after 21 cycles) than sorbents synthesised from other types of precursors.

Synthesis and calcination temperatures. Temperature is a factor that can be used to control the surface area and particle size of CaO based sorbents. Kou *et al.*⁶⁶ observed that high synthesis temperature promoted crystal growth and particle aggregation in Ca–Al mixed oxides. The average particle size of the samples also increased from 29.5 nm for the synthesised at RT to 42.1 nm for the sorbent synthesised at 80 °C. In fact, the crystallinities of CaO, Ca–Al spinel and CaCO_3 all increased with increasing synthesis temperature, as shown in Fig. 6. On the other hand, the increase in particle size is accompanied by a decrease in CO_2 capture capacity.

Apart from the temperature of the wet-synthesis, the calcination temperatures also affect the surface areas and pore volumes of the sorbents. Wang *et al.*⁶⁷ observed during the synthesis of CaO/ CaZrO_3 hollow spheres that the heating rate of calcination significantly affected the cyclic stability of the sorbent – a slow heating rate of $5 \text{ }^\circ\text{C min}^{-1}$ resulted in a stable (capacity decreased by <5 wt% after 30 cycles) compared to a sorbent prepped with a calcination rate of $20 \text{ }^\circ\text{C min}^{-1}$



Fig. 6 XRD patterns of the Ca–Al mixed oxides ($\text{Ca}^{2+}/\text{Al}^{3+} = 3$) synthesised at room temperature (RT), 60 °C and 80 °C. Reprinted with permission⁶⁶ copyright 2021 Elsevier.

(capacity decreased by <20 wt%).⁶⁷ Antzara *et al.*⁶⁸ performed the calcination of ZrO_2 promoted CaO at 750 and 800 °C and found that low calcination temperature (750 °C) reduced sintering during carbonation and resulted in CaO with high surface area and pore volume compared to CaO/ ZrO_2 sorbents calcined at 800 °C.⁶⁸

Template. The templated synthesis of CaO based sorbent has been adopted for morphology control and to introduce macro porosity to the sorbent. Carbon based template is one of the most commonly used for the synthesis of structured CaO sorbents. Ping *et al.*⁶⁹ found that the cage-like CaCO_3 hollow spheres synthesised using $\text{Ca}(\text{NO}_3)_2$, urea and polysaccharide spheres template showed an excellent CO_2 uptake of up to 78.6 wt% (100.2 mol%) in the first cycle, 45 wt% higher than the same composition synthesised without the template. Colloidal carbon spheres derived from glucose were used as the template for the synthesis of CaO/ CaZrO_3 and CaO sorbents.^{67,70} Wang *et al.*⁶⁷ found that CaO/ CaZrO_3 hollow spheres synthesised with $\text{Ca}(\text{NO}_3)_2$ and $\text{Zr}(\text{NO}_3)_4$, templated with carbon sphere (from glucose) had improved cyclic stability over 100 cycles. In a similar study, Wang *et al.*⁷⁰ prepared CaO based meshed hollow spheres by urea hydrolysis with carbon sphere (from glucose) template and demonstrated a high CO_2 capacity of ~75 wt% (96 mol%) in the first cycle, with a moderate capacity decrease of 12 wt% over 28 cycles. The authors suggested that the hollow sphere structures could produce porous CaO particles with improved CO_2 uptake.⁷⁰ In other similar studies, Naeem *et al.*⁷¹ incorporated a carbon template, prepared by poly-condensation of resorcinol with an aqueous formaldehyde solution, to the sol-gel synthesis of a Al_2O_3 and Y_2O_3 supported CaO sorbent. The resulting structure consisting of interconnected microspheres of supported CaO had an uptake of CO_2 of 61 wt% (78 mol%), which remained unchanged after 10 cycles.⁷¹

Surfactants. Previous studies have shown the use of surfactant to be an effective way to control the particle size of CaO based sorbents. In a number of cases, such as Jamrunroj *et al.*⁷²



Table 3 Various reaction conditions and capacities of MgO based sorbents^a

| Sorbent | Conditions | | | | | Capacity | | | | | | | | | | |
|-------------------------------|--|---|----------------------|---------------|--------|------------------|------------------|------------------------------|------------------------|------------------------|---------------------|---------------------------------------|------------------------|--------|-----------------|---------------|
| | Name of the sorbent | Base (B) | Promotor (P) | Fraction of S | Method | Carbonation | | Calcination temperature [°C] | Carbonation time [min] | Calcination time [min] | CO ₂ [%] | BET [m ² g ⁻¹] | CO ₂ uptake | | Cycle stability | |
| | | | | | | temperature [°C] | temperature [°C] | | | | | | [wt%] | [mol%] | | [loss%/cycle] |
| | | | | | | | | | | | | | | | | Ref. |
| MgO-AMS ₁₀ -325 °C | MgO | LiNO ₃ , KNO ₃ , Na ₂ CO ₃ , K ₂ CO ₃ | 0.44, 0.56, 0.5, 0.5 | c | 325 | 450 | 180 | 90 | HP | — | 83.9 | 76.8 | 17/30 | 88 | | |
| | MgO | LiNO ₃ , KNO ₃ , Na ₂ CO ₃ , K ₂ CO ₃ | 0.44, 0.56, 0.5, 0.5 | c | 350 | 450 | 240 | 60 | HP | — | 81.5 | 74.6 | — | 88 | | |
| | MgO | NaNO ₃ , NaNO ₂ | 0.07, 0.15 | c | 350 | 400 | 30 | 20 | Pure | 23 | 55.0 | 50.4 | 55.2/15 | 84 | | |
| | MgO | NaNO ₃ | 0.07 | c | 325 | 400 | 30 | 20 | Pure | 29 | 83.2 | 76.2 | 54.5/15 | 84 | | |
| | Mg(NO ₃) ₂ ·6H ₂ O | K ₂ CO ₃ | 3 | b | 375 | 400 | 20 | 30 | 100 | 2 | 8.6 | 7.8 | 5.1/17 | 104 | | |
| | MgO | KNO ₃ | 0.2 | c | 325 | 450 | 20 | 30 | 100 | 107 | 10.2 | 9.4 | 2412 | 105 | | |
| | MgO | KNO ₃ | 0.2 | c | 375 | 450 | 20 | 30 | 100 | 107 | 8.3 | 7.6 | 10/12 | 105 | | |
| | MgO | Na ₂ CO ₃ | 0.1 | a | 375 | 500 | — | — | Pure | — | 15.4 | 14.1 | 0/7 | 106 | | |
| | Mg(NO ₃) ₂ ·6H ₂ O | Na ₂ CO ₃ | 0.5 | b | 380 | 470 | 60 | 10 | 100 | — | 15.0 | 13.7 | —/9 | 107 | | |
| | MgO | Na ₂ CO ₃ , NaNO ₃ | 0.1 | b | 325 | 450 | 60 | 10 | Pure | 39 | 45.2 | 41.4 | 34.96/14 | 91 | | |
| MgO-AMS ₁₀ -350 °C | MgO | NaNO ₃ | 1 | b | 330 | 400 | — | — | 100 | — | 23.3 | 21.4 | —/15 | 108 | | |
| | MgO | LiNO ₃ , NaNO ₂ , KNO ₂ | 0.1 | b | 300 | 450 | 240 | 60 | HP | 19 | 73.9 | 67.7 | — | 109 | | |
| | MgO | NaNO ₃ | 0.1 | b | 350 | 350 | 30 | 30 | HP | 19 | 14.1 | 12.9 | —/20 | 109 | | |
| | MgO | NaNO ₃ | 0.1 | b | 340 | 450 | 240 | 60 | 100 | — | 69.1 | 63.3 | 14/20 | 86 | | |
| | Mg(NO ₃) ₂ ·6H ₂ O | Al(NO ₃) ₃ ·9H ₂ O | 0.3 | c | 200 | 400 | — | 60 | — | — | 3.7 | 3.3 | — | 110 | | |
| | Mg(NO ₃) ₂ ·6H ₂ O | NaNO ₃ | 0.2 | d | 300 | 450 | 180 | 60 | 100 | — | 11.5 | 10.5 | +19.02/8 | 111 | | |
| | Hydrotalcite | NaNO ₃ | 0.2 | d | 300 | 450 | 180 | 60 | 100 | — | 37.4 | 34.3 | 53.6/8 | 111 | | |
| | MgO-CeO ₂ | LiNO ₃ , KNO ₃ , Na ₂ CO ₃ , K ₂ CO ₃ | 0.17 | a | 325 | 425 | 60 | 15 | 100 | 252 | 35 | 32.1 | +1.22/30 | 112 | | |
| | Mg(NO ₃) ₂ ·6H ₂ O | Al(NO ₃) ₃ ·9H ₂ O | 1 | a | 200 | 600 | 60 | 60 | 10 | 177 | 13.1 | 12 | 12/6 | 113 | | |
| | Mg(NO ₃) ₂ ·6H ₂ O | NH ₄ OH | 5 | c | 300 | 400 | 60 | — | UP | 362 | 5.2 | 4.7 | 42/27 | 96 | | |

^a (a) Sol-gel, (b) wet mixing, (c) precipitation, (d) physical mixing, (HP) high purity, (UP) ultra purity.

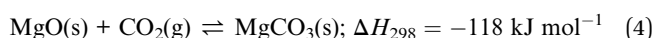
and Chen *et al.*,⁷³ there is an optimal amount of surfactant that is required to produce high performance sorbents. Jamrunroj *et al.*⁷² found that 2 mM of gemini (GS: 12-carbon hydrophobic chains and 3 carbon alkyl spacer, 12-3-12) yielded the best CO₂ capture performance. The resulting CaO-GS-2 mM sorbent, having small particles of (~37 nm) and high surface area (16 m² g⁻¹), showed the highest CO₂ uptake (29 wt% (37 mol%)) amongst all the CaO-GS sorbents tested.⁷² Similarly, Chen *et al.*⁷³ concluded that the best performing CuO/CaO sorbent was obtained with a low H₂O : cetyltrimethyl ammonium bromide (C₁₉H₄₂BrN, CTAB) molar ratio of 23 : 1. This low CTAB ratio is important for producing small particles (46.5 nm) with a CO₂ uptake of 13 wt% (17 mol%), which decreased to 10 wt% (13 mol%) after 19 cycles.⁷³ These studies exemplify that optimal levels of surfactant are crucial for producing sorbent materials with small particle sizes and high capture performance. However, in the case of CaO synthesised with sulphonic single chain (SDS), 40 mM of SDS yield the smallest particles with the lowest CO₂ uptake of 18 wt% (23 mol%) compared to other SDS doping amount.⁷² Therefore, the surfactant effect cannot be easily generalised. In addition, factors such as the micellar structures and the interfacial adsorption ability of the surfactant should also be thoroughly understood and carefully considered during synthesis.

2.3 Summary and knowledge gap

CaO based CO₂ sorbents are promising for capturing CO₂ at high temperatures. These sorbents show high CO₂ uptake capacities with rapid uptake kinetics. Significant advances have been made to improve the performance of the sorbents through carefully tuned synthetic procedures and formulations. However, major challenges remain for the efficient, robust, long term, cost-effective application of CaO based sorbents. Besides steam injection and sorbent reactivation, there are a number of synthetic approaches to enhance the uptake and cyclic stability of CaO sorbents, primarily involving supporting CaO with thermally stable support materials and optimising synthetic parameters. Challenges lie in gaining an in-depth understanding of the effectiveness of each approach, and how they can be synergistically combined to enhance the performance of the CaO sorbents. On that front, we find the use of surfactant in the synthesis of CaO sorbents a particularly interesting avenue for further research. Making good use of surfactants' surface chemistry could hold the key to producing stable, small and porous CaO particles.

3 MgO based sorbents

Magnesium oxide (MgO) captures CO₂ by:



The reversible CO₂ capture can be carried out over the temperature range between 200 and 400 °C, making it suitable for heat integration with processes where abundant low-grade heat is available. Although the maximum theoretical CO₂ uptake by MgO sorbent is high (110 wt%, 101 mol%), the

practically accessible uptake capacity is no more than 10 wt%, owing to the formation of an impermeable layer of MgCO₃, which effectively stops the encapsulated MgO from further carbonation. On the other hand, the low operating temperatures could mitigate sorbent deactivation by sintering. Therefore, the majority of the research efforts in developing synthetic MgO based sorbents focus on improving the CO₂ uptake capacities through physical and chemical modifications, including (i) introducing dopants to promote the reaction with CO₂ or (ii) preparing nanostructured MgO with very large specific surface areas to minimise the encapsulation of MgO by MgCO₃. A recent review by Hu *et al.*⁸² focuses on the development of MgO sorbent for CO₂ capture and provides a detailed insight in this topic. Here, we present a focused discussion on the synthesis and performance of these MgO sorbents. A list of recently developed MgO sorbents and their CO₂ capture performance is shown in Table 3, with key papers discussed in the following sections.

3.1 Promoted MgO sorbents

Recently, the use of alkali metal nitrates has been in the spotlight as a means to improve CO₂ capture performance of MgO based sorbents. The use of alkali metal nitrates exploits the fact that they melt during the CO₂ capture process. The molten nitrate prevents the formation of a solid MgCO₃ layer on the surface of MgO. Fig. 7 illustrates the function of the molten nitrate to promote the carbonation of MgO. The most commonly used nitrate promoters are NaNO₃ and KNO₃. Because these nitrates do not directly react with CO₂, the CO₂



Fig. 7 The role of the MgO sorbent with nitrate salts for improving CO₂ capture capacity.



capture capacity is governed by the amount of active MgO available in the solid.⁸³ In addition to alkali metal nitrates, alkali metal carbonates could also enhance the performance of MgO sorbents, rendering both faster kinetics and higher uptake capacity. Further enhancements can be achieved when carbonate and nitrate promoters are used concomitantly. These different approaches to promote MgO sorbents are discussed below.

3.1.1 Sodium nitrate (NaNO₃). The simple use of NaNO₃ as a promoter for MgO sorbent has been explored by a number of researchers. Studies using NaNO₃ as the only promoter have demonstrated effective promotional effects, reporting that doping ~7–11 mol% NaNO₃ by impregnation is the most effective in enhancing CO₂ uptake by MgO, despite the variabilities in CO₂ uptake report by different studies; the variabilities are likely to be results of the different synthesis procedures used.^{52,84,85} Zhao *et al.*⁸⁴ studied calcined mesoporous MgO, synthesised by hydrothermal process (using Mg(CH₃COO)₂ and urea), and reported the highest CO₂ uptake of 66.90 wt% (61.3 mol%) on MgO promoted with 7 mol% of NaNO₃; this is over 40 times the CO₂ uptake by pure MgO 1.28 wt% (1.2 mol%). The promotional effect was associated with the formation of triple phase boundaries between the MgO, the promoters and the gas phase.⁸⁴ With too little NaNO₃, the reaction at the phase boundaries and at the outer layer of the carbonate would be limited. In contrast, too much NaNO₃ would reduce the solubility of CO₂ as well as the contact between MgO and CO₂, thus limiting the CO₂ capture capacity.⁸⁴

3.1.2 Mixed metal nitrates. Mixed metal nitrates can also be used to create analogous promotional effects. Harada *et al.*⁸⁶ showed that 15 mol% (Li–Na–K)NO₃ on colloidal MgO nanoclusters prepared by sol–gel exhibited a high CO₂ uptake capacity of 69.10 wt% (63.3 mol%) at 340 °C. Dal Pozzo *et al.*⁸⁵ obtained promoted MgO by wet mixing commercial MgCO₃ with metal salts, followed by calcination at 450 °C. They showed that (Li, Na)NO₃, (Li, K)NO₃ and (Li, Na, K)NO₃ all promoted MgO sorbents in a similar manner to when NaNO₃ was the only promoter, reporting CO₂ uptake ~38–43 wt% (35–39 mol%). Additionally, the MgO promoted by (Li, Na, K)NO₃ showed relatively stable performance over 10 cycles.

3.1.3 Nitrites. The use of nitrites can be an alternative or complement to nitrate promoters. In addition to using nitrates, Harada *et al.*⁸⁶ promoted colloidal MgO nanoclusters with LiNO₂–(Na–K)NO₂. The nitrite-promoted MgO sorbent had a CO₂ uptake of 68.2 wt% (62.4 mol%) at 340 °C, with better cyclic stability than the MgO promoted by (Li–Na–K)NO₃ (Fig. 8). Zhao *et al.*⁸⁴ showed that using a mixture of nitrate and nitrite promoters can further enhance the performance of the hydrothermally synthesised MgO sorbents.⁸⁴ When 0–8 mol% NaNO₂ was doped to NaNO₃-promoted MgO (with molar ratio of MgO : NaNO₃ = 1 : 0.07) the CO₂ uptake increased from 66.9 wt% (61.3 mol%) to over 87 wt% (80 mol%), whilst showing stable performance over 15 cycles.

3.1.4 Carbonates. The presence of a carbonate promoter facilitate easier melting and faster CO₂ transport through the carbonate layer. Kwak *et al.*⁸⁷ employed a triple eutectic alkali carbonate (TEC) design, in which the MgO sorbent was



Fig. 8 CO₂ capture capacity of promoted MgO by alkali metal nitrates ((Li–Na–K)NO₃) and nitrate/nitrite (LiNO₃–(Na–K)NO₂) salt. Reprinted with permission⁸⁶ copyright 2021 American Chemical Society.

promoted by a TEC mixture consisting of Li₂CO₃, Na₂CO₃, and K₂CO₃ (with a molar ratio of Li : Na : K of 0.435 : 0.315 : 0.250). They classified the CO₂ capture process into two steps: (1) “fast and large”, and (2) “slow and small”. The amount of TEC used affects the kinetics of these two steps differently – the rate of step 1 increases with increasing amount of TEC; but this was not observed for step 2. The optimal TEC amount was found to be 60 mol% (sample 60-TEC/MgO), which gave a CO₂ uptake of 43.4 wt% (39.7 mol%) in step 1 and an additional 33.9 wt% (31.0 mol%) in step 2. It was also found that MgO with low TEC content (20–40 mol%) had better cyclic stability than those with high TEC content (60–100 mol%).

3.1.5 Carbonates with nitrite or nitrate. Co-Doping of carbonates and nitrates has been a popular approach for developing promoted MgO based sorbents,^{83,88–91} with key studies summarised in Table 3. Here, we discuss key synthetic parameters governing the performance of the co-doped sorbents. Hwang *et al.*⁸³ investigated the doping of K₂CO₃ to NaNO₃ and KNO₃-promoted commercial MgO and found the K₂CO₃ : nitrate ratio to be important. Co-doping 30 wt% K₂CO₃ with 10 wt% of NaNO₃ or KNO₃ both worked well, rendering 44 wt% (40 mol%) uptake at 300 °C in 20 atm CO₂.⁸³ Vu *et al.*⁹¹ promoted the performance of mesoporous MgO aerogels with double sodium salts (MgO·Na₂CO₃·NaNO₃). During operation, Na₂CO₃ and NaNO₃ facilitate a high concentration of O^{2–} in the molten salts, which would enhance the CO₂ capture capacity by accelerating the formation of MgCO₃. Furthermore, the molten salts hinder the



formation of the rate-limiting carbonate surface layers, whilst accelerating the production of CO_3^{2-} . Therefore, it is important to dope MgO with an optimal amount of alkali salts to maximise the benefit of eutectic formation. Specifically, the amount of Na_2CO_3 should be equal to or less than the amount of NaNO_3 for optimal CO_2 capture performance. According to Vu *et al.*, the highest CO_2 uptake of 56 wt% (51 mol%) was achieved at 325 °C (1 atm, pure CO_2) when the molar ratio of $\text{MgO} : \text{Na}_2\text{CO}_3 : \text{NaNO}_3$ was 1 : 0.05 : 0.2.⁹¹ Wang *et al.*⁹² also showed the benefit of having both nitrate and carbonate doped on MgO nano-sheets through a series of experiments and found that the optimal sorbent composition to be $[(\text{LiNO}_3, \text{KNO}_3)_2 - (\text{Na}_2\text{CO}_3, \text{K}_2\text{CO}_3)]_{0.15} / \text{MgO}$, which showed a high CO_2 uptake of 73 wt% (67 mol%) (350 °C, 1 atm, 100% CO_2). They proposed a reaction mechanism between CO_2 and the sorbent, involving the following steps:



The finding of Wang *et al.*⁹² was in agreement with Ding *et al.*,⁸⁸ who revealed that the reaction between CO_2 and MgO promoted with 10 mol% $[(\text{Li}_{0.44}\text{K}_{0.56})\text{NO}_3]_2[(\text{Na}_{0.5}\text{K}_{0.5})\text{CO}_3]$ takes place in three stages: (1) the formation of carbonate in the first 7 minutes – at this stage, CO_2 is dissolved in the molten salt and then reacts with MgO and formed a layer of carbonate (CO_3^{2-}), producing $\text{K}_2\text{C}_2\text{O}_6$ and $\text{K}_2\text{Mg}(\text{CO}_3)_2$. (2) The restriction of the rigid carbonate layer and the formation of the high concentration of oxygen ion within 10 minutes – oxygen ions (O^{2-}) are produced by the dissolution of MgO and the decomposition of the molten alkali nitrates and nitrites. (3) The nucleation of magnesium carbonate occurs between 10 and 60 minutes after contacting the CO_2 .

3.2 Structured MgO sorbents

Morphological features, such as surface area, pore volume, size and thickness of the particle are all critical to the performance of MgO sorbents.⁹³ Therefore, researchers have explored various synthetic approaches to improve the morphological properties of MgO sorbents to enhance their CO_2 uptake.^{94–96} In general, the CO_2 uptake correlates well to the sorbent's surface area. Guo *et al.*⁹⁴ showed that solid state chemical reaction (SR) method produced MgO with, smaller particle sizes, higher BET surface area ($100 \text{ m}^2 \text{ g}^{-1}$), smaller pore sizes and higher pore volume ($0.67 \text{ cm}^3 \text{ g}^{-1}$) than those produced by other synthesis methods, such as direct calcination (DC), direct precipitation (DP) and sol-gel (SG) – when MgCl_2 was used as the Mg precursor in all the synthesis methods. As a result, MgO synthesised by SR showed higher CO_2 uptake (10.5 wt%, 9.6 mol%) than those by the DC, DP and SG methods, which yielded CO_2 uptakes of 2.95–6.8 wt% (2.7–6.2 mol%). In addition, the CO_2 capture capacities are also correlated to the sorbents' basicity, which are classified as weak, medium and strong. Accordingly, the SR method yielded the highest number of medium and strong basic sites (responsible for 2.54 and 1.24 mmol CO_2 per g of uptake, respectively) as well

as the highest total amount of basic sites (with a total uptake of 5.49 mmol CO_2 per g). The abundant basic sites enhanced the CO_2 uptake of the SR sorbent. Similarly, Ding *et al.*⁹⁵ showed that MgO synthesised from magnesium acetate tetrahydrate ($\text{Mg}(\text{CH}_3\text{COO})_2$) and oxalic acid ($\text{C}_2\text{H}_2\text{O}_4$) dihydrate solution (MgO–MO) had a high BET surface area of $252 \text{ m}^2 \text{ g}^{-1}$, high pore volume of $0.763 \text{ cm}^3 \text{ g}^{-1}$ and CO_2 uptake capacity of 7.59 wt% (7.0 mol%) at 50 °C. The CO_2 uptake capacity of MgO–MO was superior compared to MgO synthesised by calcining magnesium carbonate (MgO–BMC), the rehydration of MgO–BMC (MgO–RF) and commercial MgO (MgO–CA).⁹⁵ Hanif *et al.*⁹⁶ found that MgO obtained by ammonia precipitation (AC) showed higher surface area ($362 \text{ m}^2 \text{ g}^{-1}$, $0.701 \text{ cm}^3 \text{ g}^{-1}$) and CO_2 uptake 7.53 wt% (6.9 mol%) than those by urea hydrolysis (UC) and thermal degradation (TC).

Researchers have also developed porous MgO with structural regularities as a means to control the morphologies of the synthetic sorbents. The performance of the various MgO sorbents with well-defined morphologies is summarised in Fig. 9. Notable morphologies are discussed in details below (Fig. 10).

3.2.1 Sheets. Wang *et al.*⁹² synthesised sheet-like $[(\text{Li}, \text{K})_2 - (\text{Na}, \text{K})]_{0.15} / \text{MgO}$ having a sheet thickness of $\sim 40 \text{ nm}$. The MgO nanosheets showed higher CO_2 uptake than granular MgO because the former had more surface MgO, which can readily react with CO_2 . This advantage is corroborated by the nanosheets' larger BET surface area ($56 \text{ m}^2 \text{ g}^{-1}$), larger pore volume ($0.24 \text{ cm}^3 \text{ g}^{-1}$) and larger mean pore diameter than the granular MgO. Additionally, the sheet-like MgO sorbents showed relatively stable performance over 20 cycles. CO_2 uptake capacity is summarised by the morphology with the surface area in Fig. 9.

3.2.2 Platelets. Hanif *et al.*⁹⁶ prepared both platelet, sheet-like and octahedra structured MgO sorbents. They found that platelet morphology shows larger BET surface area ($362 \text{ m}^2 \text{ g}^{-1}$), higher pore volume ($0.701 \text{ cm}^3 \text{ g}^{-1}$) and relatively higher CO_2 uptake of 7.53 wt% (6.9 mol%) than the other two morphologies.

3.2.3 Rods. Zhao *et al.*⁸⁴ and Tuan *et al.*⁹⁷ found rod-like MgO to perform better than other tested shapes such as MgO spheres (they are described as 'ball-like' in the original paper).

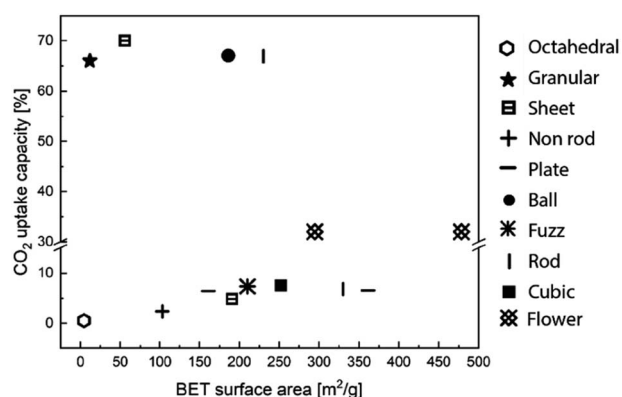


Fig. 9 CO_2 uptake capacity and BET surface area according to the various structure of MgO sorbents. The data points entries are obtained from ref. 84, 92, 95, 96, 98 and 99.





Fig. 10 SEM images of the structure of MgO sorbents: plate,⁹⁶ rod,⁹⁷ and fuzzi-like structure of MgO sorbents⁹⁵ and TEM image of the flower-like plate.⁹⁸ Reprinted with permission copyright 2021 American Chemical Society.⁹⁶ Reprinted with permission copyright 2021 Royal Society of Chemistry.⁹⁵ Reprinted with permission copyright 2021 John Wiley and Son, Inc.^{97,98}

Both teams attributed the enhanced CO₂ uptake by the rod-like MgO to their high BET surface area (230–331 m² g⁻¹), larger pore volume (0.49–0.58 cm³ g⁻¹) as well as small particle sizes (~7 nm in both studies). CO₂ uptake capacity of rod-like MgO are drawn in Fig. 9.

3.2.4 Cubes. Cubic morphology may not be a trivial morphology that is typically associated with high specific surface areas. However, Ding *et al.*⁹⁵ reported a sorbent consisting of cube-like MgO grains with high BET surface area and pore volume (252 m² g⁻¹, 0.76 cm³ g⁻¹). The MgO microcubes showed a CO₂ uptake capacity of 7.59 wt% (7.0 mol%), outperforming the plate-like MgO 6.44 wt% (5.9 mol%) prepared in the same study. Both of CO₂ uptake capacity are added in Fig. 9.

3.2.5 Flower. Li *et al.*^{98,99} synthesised MgO/C composites with flower-like morphology. The large surface area and pore volume (295 m² g⁻¹, 0.94 cm³ g⁻¹)⁹⁸ of the flower-like morphology facilitated efficient mass transport and improved the CO₂ uptake capacity of the MgO sorbents. Experimentally, the MgO/C nanocomposite showed a high CO₂ uptake of 30.9 wt% (28.3 mol%) at 27 °C, 1 bar. Using a similar synthetic strategy, Li *et al.*¹⁰⁰ combined the flowerlike MgO/C with the sheet-like graphene oxide and produced a sandwich-like structure with surface area (478 m² g⁻¹) and pore volume (1.22 cm³ g⁻¹) even higher than the graphene oxide-free MgO/C nanocomposite. The sandwich-like structured showed an apparent uptake capacity of 31.5 wt% (28.8 mol%),¹⁰⁰ also plotted in Fig. 9.

3.3 Summary and knowledge gap

MgO based materials are promising CO₂ sorbents for applications at moderately high temperatures. When low-grade heat (<400 °C) is abundantly available on-site, using MgO to capture CO₂ may be more advantageous than calcium looping.¹⁰¹ Additionally, MgO has the potential to become a highly effective CO₂

sorbent if its stoichiometric capture capacity can be fully exploited. In practice, the performance of MgO based sorbents is significantly hindered by its unfavourable carbonation mechanism and sluggish rates. Many different approaches have been studied to promote the uptake of CO₂ by MgO. Whilst high surface area, morphologically well-defined MgO sorbents could significantly improve CO₂ uptake, the experimentally accessible capacities are still substantially lower than the CaO based sorbents. Also, carbonation–calcination cycles could induce drastic morphological changes to the sorbents, making the morphologies of the freshly-prepared materials less relevant to the long-term performance.¹⁰² Alternatively, the doping of alkaline metal salts to form low-melting eutectics is a much more effective to tackle the issue of the slow CO₂ uptake kinetics. However, the underlying science governing the promotional effects, including the interaction between the different salts in the eutectics, the interplay between different phases (*e.g.* molten salt, MgO and MgCO₃) and the mechanisms of ionic diffusion in the molten salt, must be further studied and better understood.¹⁰³ Lastly, many MgO sorbents suffer from poor cyclic stability. Therefore, further development is required to improve the effectiveness of the MgO based sorbents.

4 Li, Na, K, Sr and Ba based sorbents

As briefly discussed in Section 1, the carbonation of Li₂O, Na₂O, K₂O, SrO and BaO is practically irreversible. However, irreversible CO₂ sorbents are economically unattractive as they cannot be recycled and reused in continuous processes. Therefore, Li, Na, K, Sr and Ba based sorbents are often formulated as ternary oxides consisting of (i) at least one alkali metal or alkaline earth metal and (ii) at least one transition metal or semi-metal. The presence of transition metals and semi-metals introduces acidity to the ternary oxides and modulates the overall basicity of the sorbents, making them thermally regenerable at practically achievable temperatures. This section discusses the recent

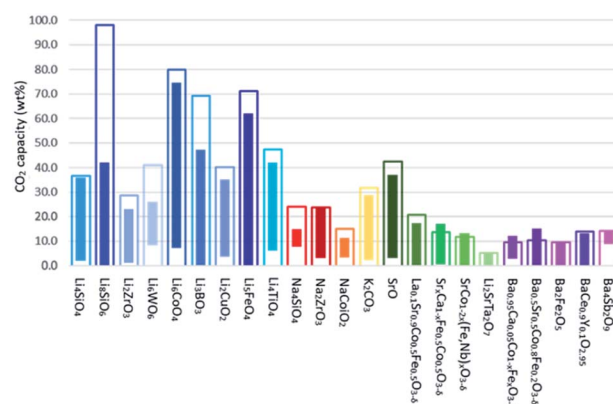


Fig. 11 Theoretical and experimental CO₂ uptake capacities of various Li-, Na-, K-, Sr- and Ba- based CO₂ sorbents. The hollow bars represent the stoichiometric capture capacities, whereas the solid bars represent the range of experimentally measured CO₂ uptakes. The sorbents are classified according to the chemical composition of the active components, *i.e.* excluding the formulation of the support.





Table 4 Various reaction conditions and capacities of Li, Na, K, Sr and Ba based sorbents^a

| Sorbent | Synthesis method | BET [m ² g ⁻¹] | Stoichiometric CO ₂ capacity [wt%] | Experimental CO ₂ uptake | | Carbonation temperature [°C] | Calcination temperature [°C] | Carbonation CO ₂ partial pressure [bar] | Calcination CO ₂ partial pressure [bar] | Max no. of cycles | Ref. |
|--|------------------|---------------------------------------|---|-------------------------------------|------------|------------------------------|------------------------------|--|--|-------------------|-----------------|
| | | | | [wt%] | [mol%] | | | | | | |
| Li ₄ SiO ₄ | a, b, c | 0.06–10 | 36.7 | 1.8–36.0 | 4.9–98.1 | RT–700 ^b | 550–900 | 0.04–1.0 | 0 | 250 | 114 and 116–121 |
| Li ₈ SiO ₆ | a | — | 98.0 | 0–42.0 | 0–42.9 | 25–776 ^b | — | 1.5 | — | — | 115 |
| Li ₂ ZrO ₃ | a, b, c | 2–3 | 28.7 | 0.01–23.0 | 0–80.1 | 500–575 | 600–700 | 0.10–2.0 | 0–0.585 | 30 | 122–124 |
| Li ₆ WO ₆ | a | 8 | 41.1 | 3.6–25.9 | 8.8–63.0 | 30–710 ^b | 730–760 | 0.60 | 0 | 4 | 130 |
| Li ₆ CoO ₄ | a | 1 | 80.0 | 5.0–76.4 | 6.3–95.5 | 300–700 | 700–750 | 0.20–1.0 | 0 | 10 | 127 |
| Li ₃ BO ₃ | c, d | 1–3 | 69.1 | 0–47.2 | 0–68.3 | 500–650 | 650 | 0.20–1.0 | 0 | 10 | 131 |
| Li ₂ CuO ₂ | a, c | 1–6 | 40.2 | 3.6–37.4 | 9.0–93.0 | 30–750 ^b | 750–850 | 1.0–5.0 | 0 | — | 128 and 129 |
| Li ₅ FeO ₄ | a | — | 71.2 | 0–62.0 | 0–87.1 | 30–700 ^b | — | 1.0 | — | — | 126 |
| Li ₄ TiO ₄ | a | — | 47.3 | 0–42.0 | 0–88.8 | 300–856 | — | 1.0 | — | — | 125 |
| Na ₄ SiO ₄ | d | — | 23.9 | 7.7–19.2 | 32.2–80.3 | 50–840 ^b | — | 0.80 | — | — | 133 |
| Na ₂ ZrO ₃ | a, d | 4–5 | 23.8 | 4.5–23.8 | 18.9–100.0 | 150–800 | 680–900 | 0.025–1.0 | 0 | 70 | 134–137 |
| NaCoO ₂ | a | — | 15.0 | 3.3–11.1 | 22.0–73.3 | 100–800 | — | 0.050–1.0 | — | — | 132 |
| K ₂ CO ₃ | b, c, e | 0.4–459 | 31.8 | 4.3–28.7 | 13.5–90.3 | 50–100 | 60–300 | 0.010–0.18 | 0–1.0 | 10 | 138–143 |
| SrO | e | 1–3 | 42.5 | 3.0–37.1 | 7.1–87.3 | 1100–1200 | 1100–1200 | 0.30–0.50 | 0 | 10 | 144 |
| La _{0.1} Sr _{0.5} Co _{0.5} Fe _{0.5} O _{3–δ} | f | — | 20.7 | 0–17.3 | 0–83.6 | 600–800 | — | 0.10–1.0 | — | — | 145 |
| Sr _x Ca _{1–x} Fe _{0.5} Co _{0.5} O _{3–δ} | f | — | 27.3 | 0.4–17.0 | 1.5–62.3 | RT–950 ^b | — | 1.0 | — | — | 146–148 |
| SrCo _{1–2x} (Fe, Nb) _x O _{3–δ} | a | — | 23.6 | 0–13.1 | 0–55.5 | 925 | — | 0.75 | — | — | 149 |
| Li ₂ SrTa ₂ O ₇ | — | — | 5.1 | 0–4.9 | 0–96.1 | 140 | 700 | — | — | 6 | 151 |
| Ba _{0.95} Ca _{0.05} Co _{1–x} Fe _x O _{3–δ} | f | — | 19.2 | 2.8–12.0 | 14.6–62.5 | 850 | — | 0.10 | — | — | 148 |
| Ba _{0.5} Sr _{0.5} Co _{0.5} Fe _{0.2} O _{3–δ} | a | — | 20.9 | 0–14.9 | 0–71.4 | RT–950 ^b | — | 1.0 | — | — | 149 |
| Ba ₂ Fe ₂ O ₅ | a | — | 18.8 | 0–9.4 | 0–50.0 | 1000 | 1000 | 1.0 | 0 | — | 153 and 154 |
| BaCe _{0.9} Y _{0.1} O _{2.95} | a | — | 13.8 | 0–13.1 | 0–94.9 | 600–1000 | — | 1.0 | — | — | 152 |
| Ba ₄ Sb ₂ O ₉ | a | — | 14.1 | 9.5–14.0 | 67.4–99.3 | 650–750 | 950 | 0.42 | 1 | 100 | 155 |

^a Synthesis methods: (a) solid state; (b) impregnation suspension; (c) doping; (d) wet chemistry; (e) calcination; (f) citrate sol–gel method. ^b Indicates temperature programmed CO₂ capture experiments in a TGA.



Fig. 12 (a) Schematic illustration of the "double shell" model describing Li_4SiO_4 carbonation. Reprinted with permission¹¹⁴ copyright 2021 John Wiley and Son, Inc. (b) Temperature-programmed carbonation of Li_8SiO_6 in a TGA. Reprinted with permission¹¹⁵ copyright 2021 American Chemical Society. (c) Illustration of synthesis of Li_6WO_6 NWs and its morphological change 30 min of carbonation at 700 °C. Reprinted with permission⁹¹ copyright 2021 American Chemical Society. (d) Schematic illustration of CO_2 capture and release on Li_6WO_6 NWs under dry and wet conditions. Reprinted with permission¹ copyright 2021 American Chemical Society.

development in the formulation, synthesis and the CO_2 capture performance of synthetic Li, Na, K, Sr and Ba based sorbents. Fig. 11 summarises the stoichiometric and experimental CO_2 uptake capacities of the Li, Na, K, Sr and Ba based sorbents reported in the recent literature. A more elaborated summary is provided in Table 4.

4.1 Li based sorbents

4.1.1 Lithium silicates. Lithium silicates, including Li_4SiO_4 and Li_8SiO_6 , are considered to be the most studied lithium based sorbents. The carbonation mechanism of these ternary oxides are fundamentally different from the CaO and MgO based ones, as more than one solid phases will form during carbonation. Li_4SiO_4 reacts with CO_2 between 450 and 700 °C with a stoichiometric CO_2 uptake capacity of 36.7 wt% according to:



The two solid products arrange themselves following a double-shell model, in which Li_2CO_3 and Li_2SiO_3 form an outer shell and an inner shell, respectively, as depicted in Fig. 12a.¹¹⁴ The inner Li_2SiO_3 shell encapsulates the unreacted Li_4SiO_4 core. Once the shells have fully developed, further

carbonation requires the migration of CO_2 inward through the Li_2CO_3 layer, and the migration of Li^+ and O_2^- ions outward through the Li_2SiO_3 layer. Therefore, the interface between Li_2CO_3 and Li_2SiO_3 is regarded as the reaction front, where new Li_2CO_3 forms. As both shells grow thicker, the diffusion resistance increases and slows down the rate. It is believed that the diffusion of CO_2 through the Li_2CO_3 layer is the rate limiting step, because the diffusion of CO_2 through the carbonate is considered slower than the diffusion of Li^+ and O_2^- through the silicate. Owing to the product layer diffusion resistances, the experimentally accessible uptake capacities are always lower than the stoichiometric values. For the chemically unmodified lithium silicates, the surface area of the sorbent becomes the effective rate limiting factor, which subsequently determines the practically achievable uptake capacity.

Using a lithium-rich compound such as Li_8SiO_6 could potentially improve the CO_2 uptake to 98 wt%. The carbonation of Li_8SiO_6 consists of 3 steps, as illustrated in Fig. 12b and confirmed by *in situ* synchrotron powder X-ray diffraction (SPXRD):¹¹⁵

Steps 1 and 2 involve the uptake of CO_2 by Li_8SiO_6 on the surface and in the bulk:



Step 3 involves the uptake of CO₂ by the formed Li₄SiO₄:



Lithium silicates can be easily synthesised by solid-state reactions. A typical synthesis involves mechanically mixing lithium and silicon precursors with desired stoichiometric ratios, followed by drying and calcination (at 800–900 °C). Typical lithium precursors include Li₂CO₃,^{116,117} Li₂O (ref. 118) and LiNO₃,¹¹⁹ whereas the silicon precursor is almost always SiO₂. Regardless of the precursor used, solid-state synthesised lithium silicates exhibit low specific surface areas (<1 m² g^{−1}) and low experimental CO₂ uptake capacities: 28–35 wt% (76–95 mol%) for Li₄SiO₄ (ref. 116 and 117) and 42 wt% (43 mol%) for Li₈SiO₆.¹¹⁵ In addition, the poor sintering resistance of the solid product, Li₂SiO₃, results in rapid performance decay over CO₂ capture cycles.¹¹⁷

Given the dependence on product layer diffusion during carbonation, it is intuitive to prepare Li₄SiO₄ sorbents with high surface areas using wet chemistry methods such as impregnation suspension,^{114,120} which involves mixing an aqueous solution of lithium precursors (e.g. lithium acetate and lithium lactate) with a SiO₂ sol suspension, which is subsequently dried and calcined.¹¹⁴ Indeed, the resulting Li₄SiO₄ samples exhibit higher surface areas (1.6–2 m² g^{−1}), higher CO₂ uptake (up to 36 wt%, i.e. 98 mol%) and better cyclic durability (over 40 cycles) than those synthesised by solid-state reactions.¹¹⁴

Alternatively, the performance of Li₄SiO₄ can be improved by doping. Inert dopants (e.g. CaCO₃) can increase the sorbents' specific surface area and sintering resistance.¹¹⁷ Low melting-point dopants, e.g. Na₂CO₃, K₂CO₃, NaNO₃ and KNO₃, can accelerate the transport of CO₂ through the Li₂CO₃ product layer, analogous to the case of alkali metal salt doped MgO sorbents.^{119–121} Lastly, redox-active dopants, such as Fe³⁺, can improve the transport of O^{2−} ions through the Li₂SiO₃ product layer.¹¹⁸ Synthetically, doping can be achieved by including dopant precursors during the solid state synthesis of the Li₄SiO₄ sorbent,^{116,117} impregnating the solid-state synthesised Li₄SiO₄ with soluble dopants (e.g. Na₂CO₃, K₂CO₃, NaNO₃ and KNO₃), or performing a secondary solid state reaction between the as-synthesised Li₄SiO₄ and the dopant precursor. Two-step solid state synthesis was used for the synthesis of Li_{4+x}Si_{1−x}Fe_xO₄ sorbents from Li₄SiO₄ and Li₅FeO₄.¹¹⁸ As an economic and sustainable alternative, Wang *et al.* used acid-leached blast

furnace slag, which contains TiO₂, Fe₂O₃, Al₂O₃, CaO and K₂O, as the silicon precursor for the solid-state synthesis of Li₄SiO₄.¹¹⁶ The inherent presence of dopants in the silica precursor offers a cost-effective means to prepare high performance Li₄SiO₄ sorbents. In all cases, the dopant-promoted Li₄SiO₄ showed increased specific surface area (from 0.06 to 0.3 m² g^{−1}), improved CO₂ uptake (up to 35 wt%, i.e. 95 mol%),¹¹⁷ improved cyclic stability (up to 250 cycles)¹²¹ and faster rate of carbonation at low reaction temperatures in low CO₂ concentrations (in 20% CO₂ at 200 °C).¹¹⁸

4.1.2 Other Li based sorbents. Lithium zirconate (Li₂ZrO₃) is the second most studied lithium based sorbent with a stoichiometric uptake capacity of 28.7 wt%:



The experimentally reported carbonation temperatures are in the range of 450–650 °C. Similar to lithium silicates, the carbonation of Li₂ZrO₃ also proceeds *via* a double shell model, in which the inner and outer product layers are ZrO₂ and Li₂CO₃, respectively. The CO₂ diffusion through the Li₂CO₃ inner layer is considered to be the rate limiting step. Li₂ZrO₃ can be simply synthesised by solid-state reaction from Li₂CO₃ and ZrO₂. However, solid-state synthesised Li₂ZrO₃ show slow carbonation and low uptake capacities (5.9–10 wt%, i.e. 20.6–34.8 mol%).^{122,123} Therefore, synthetic methods used to improve the performance of Li₄SiO₄ have also been adopted to promote the Li₂ZrO₃ sorbents, such as (i) doping low-melting point salts to improve the CO₂ mobility through the carbonate product layer,¹²³ (ii) doping redox-active Fe³⁺ to improve the O₂[−]–CO₃^{2−} bi-ionic diffusivity through the Li₂CO₃ product layer,¹²² and (iii) preparing Li₂ZrO₃–Na₂ZrO₃ solid-solution sorbents by impregnation suspension.¹²⁴ Methods (i) and (iii) appear to be more effective in enhancing CO₂ uptake (20–22 wt%, i.e. 70–77 mol%), whereas the improvement by Fe-doping is marginal (7.0–9.2 wt%, i.e. 24.4–32.1 mol%).

Ternary oxide phases containing Li and transition metals have also been prepared, primarily by solid-state synthesis, as CO₂ sorbents.^{125–130} A summary of the carbonation chemistries of these Li-transition metal oxides is presented in Table 5. Amongst these ternary oxides, Li₆CoO₄ has both the highest stoichiometric CO₂ uptake and the highest experimental CO₂ uptake of 80.0 and 74.5 wt%, respectively,¹²⁷ whereas Li₆WO₆ nanowires showed the ability to rapidly capture CO₂ at ambient

Table 5 Summary of carbonation reactions of Li-transition metal-oxide materials

| Active sorbent | Carbonation reactions | Stoichiometric CO ₂ uptake capacity (wt%) |
|----------------------------------|---|--|
| Li ₄ TiO ₄ | Li ₄ TiO ₄ + 4CO ₂ = 4Li ₂ CO ₃ + TiO ₂ | 41.5–47.3 |
| Li ₃ FeO ₄ | Li ₃ FeO ₄ + 2CO ₂ = LiFeO ₂ + 2Li ₂ CO ₃ | 71.2 |
| | LiFeO ₂ + CO ₂ = Li ₂ CO ₃ + Fe ₂ O ₃ | |
| Li ₆ CoO ₄ | Li ₆ CoO ₄ + 3CO ₂ = 3Li ₂ CO ₃ + CoO | 80 |
| Li ₂ CuO ₂ | Li ₂ CuO ₂ + CO ₂ = Li ₂ CO ₃ + CuO | 40.2 |
| Li ₆ WO ₆ | Li ₆ WO ₆ + CO ₂ = Li ₄ WO ₅ + Li ₂ CO ₃ | 41.1 |
| | Li ₄ WO ₅ + CO ₂ = Li ₂ WO ₄ + Li ₂ CO ₃ | |
| | Li ₂ WO ₄ + CO ₂ = WO ₃ + Li ₂ CO ₃ | |



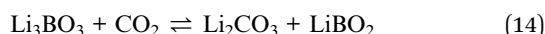
temperatures in the presence of moisture (relative humidity = $58 \pm 3\%$). The high performance of Li_6WO_6 nanowires at ambient temperatures is attributed to the hydration and activation of the surface of the nanowires for accelerated carbonation, as illustrated in Fig. 12d.¹²⁷ For sorbents containing redox-active metals, *e.g.* Co and Fe, the redox environment during carbonation will also affect the CO_2 capture performance. For instance, the presence of O_2 promotes CO_2 uptake of Li_5FeO_4 by enhancing the ionic diffusion through the product layer.¹¹⁸ In contrast, the performance of Li_6CoO_4 deteriorates quickly over cycles (76.4 wt%, *i.e.* 95.5 mol%, in the first cycle to 30.5 wt%, *i.e.* 38.1 mol% after 10 cycles), owing to the irreversible oxidation of Co^{2+} to Co^{3+} by the O_2 present under the testing conditions.¹²⁷

The cyclic stability of Li-transition metal oxides is either poor or unreported. Doping a second transition metal (*e.g.* Mn, Fe or Ni)¹²⁸ and alkali metal nitrates (MNO_3 , $\text{M} = \text{Li, Na, K}$)¹²⁹ has been proven effective for improving the capture capacity (from 23 wt% to 35 wt%, *i.e.* 57 to 87.1 mol%) and cyclic stability of Li_2CuO_2 . Again, the improvement is by virtue of improving the ionic conductivity of the product layers.

Lastly, trilithium borate (Li_3BO_3) has been synthesised by precipitation using LiOH and H_3BO_3 as the precursors.¹³¹ Li_3BO_3 captures CO_2 with a stoichiometric uptake capacity of 41.4 wt%:



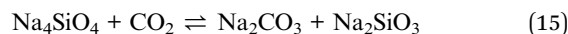
With a reported experimental CO_2 uptake of 35.4 wt% (51.2 mol%), measured after 4 h in pure CO_2 at 580°C . The poor cyclic stability of Li_3BO_3 could be improved by NaNO_2 or KNO_2 doping, which significantly accelerates product layer diffusion as the dopant salts form a molten layer. Interestingly, the 10 mol% (Na-K) NO_2 doped Li_3BO_3 showed an experimental uptake of 47.2 wt% (68.3 mol%), exceeding the stoichiometric maximum capacity predicted by eqn (16). This was because the alkali metal nitrites promoted the deep carbonation of lithium borate:



Resulting in improved stoichiometric uptake capacities of 69.1 and 55.4 wt%, respectively.

4.2 Na based sorbents

Na based sorbents have similar chemical formulae as the Li based ones (see Section 4.1). Because sodium is earth-abundant, Na based sorbents are potentially more economical. On the other hand, sodium is heavier and therefore, the stoichiometric CO_2 uptake capacity of Na based sorbents are generally lower than that of the Li equivalents in terms of wt%. Experimentally, sodium orthosilicate, sodium zirconate and other sodium metal oxides have shown promising CO_2 capture performance over a wide temperature range (from near-ambient temperatures to 850°C):



These compounds generally exhibit good cyclic stability, with the exception of undoped Na_2CoO_2 :



which shows limited experimental CO_2 uptake (3.3–5.0 wt%, *i.e.* 22.0–33.3 mol%) that is substantially below the stoichiometric capacity of 15 wt%.¹³²

Similar to Li based sorbents, Na based sorbents can be prepared by solid-state reactions between metal precursors, *e.g.* $\text{Na}_2\text{SiO}_3 + \text{NaOH}$,¹³³ $\text{Na}_2\text{CO}_3 + \text{ZrO}_2$,¹³⁴ and $\text{Na}_2\text{CO}_3 + \text{CoCO}_3$,¹³² as well as by wet-chemistry methods such as sol-gel synthesis.^{135,136}

Na_4SiO_4 was found to perform well above 750°C , showing a maximum uptake of 19.2 wt% (80.3 mol%, with a stoichiometric uptake capacity of 23.9 wt%) at 840°C .¹³³ One approach to improve the low-temperatures performance of Na_4SiO_4 is doping alkali carbonates (M_2CO_3 , $\text{M} = \text{Li, Na, K}$), which promotes the diffusion of O_2^- through the molten carbonate layer. The promotional effects follow the order $\text{K}_2\text{CO}_3 > \text{Na}_2\text{CO}_3 > \text{Li}_2\text{CO}_3$, probably because of the increased basicity from Li to K.¹³³ Although the dopants decrease the mass-based CO_2 uptake capacity of the Na_4SiO_4 sorbent, doping significantly improved carbonation rates even below 700°C . In particular, K_2CO_3 -doped Na_4SiO_4 showed 4.7 wt% (19.7 mol%) CO_2 uptake at 300°C , doubling that of undoped Na_4SiO_4 .

During the carbonation of Na_2ZrO_3 , the solid products could form a mesoporous layer with high gas permeability, as depicted in Fig. 13a and b. As a result, the Na_2ZrO_3 sorbents do not



Fig. 13 (a) Scheme of the CO_2 uptake on Na_2ZrO_3 at different temperatures. Reprinted with permission¹³⁴ copyright 2021 American Chemical Society (b) SEM image of growth of ZrO_2 and Na_2CO_3 after the carbonation of Na_2ZrO_3 . Reprinted with permission¹³⁴ copyright 2021 American Chemical Society (c) Scheme of the CO_2 and sodium diffusion in the sorbent under fresh and sintered state. Reprinted with permission¹³⁵ copyright 2021 Elsevier.

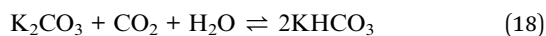


experience significant product layer diffusion resistance, as long as the product layer does not sinter.¹³⁷ Nevertheless, increasing the initial porosity of Na_2ZrO_3 , *e.g.* by synthesising the sorbent using sol-gel method, could still render improvements in CO_2 uptake and cyclic stability during high temperature operations.¹³⁵ The best performance was achieved by the Na_2ZrO_3 prepared from sodium oxalate and $\text{Zr}(\text{NO}_3)_4$, showing an uptake of 22.6 wt% (95.0 mol%, with a stoichiometric uptake of 23.8 wt%), which was largely maintained over 5 successive cycles. Ji *et al.* attributed the high performance to the partly sintered product layer, which facilitates fast sodium diffusion as a form of mass transfer enhancement, as depicted in Fig. 13c.

For NaCoO_2 , substitutionally doping the Co sites with Fe could substantially improve the redox activity, ionic conductivity and therefore CO_2 capture performance of the ternary oxide. For instance, $\text{NaCo}_{0.7}\text{Fe}_{0.3}\text{O}_2$ showed improved capacity of 10.6 wt% (70.7 mol%) in 20% CO_2 at 700 °C (*cf.* 3.3 wt%, 22.0 mol% without doping).¹³² The CO_2 uptake could be further improved to 11.1 wt% (74.0 mol%) in the presence of 5% O_2 at 800 °C, because the presence of O_2 would stabilise the NaCoO_2 phase.

4.3 K based sorbents

Unlike lithium and sodium based sorbents, whose functional forms are mixed oxides, potassium based sorbents primarily function in the form of K_2CO_3 and take up CO_2 by forming bicarbonate in the presence of moisture with a stoichiometric CO_2 uptake capacity of 31.8 wt%:



Experimentally, the carbonation and regeneration of K_2CO_3 occur at 50–60 °C and around 200 °C, respectively. This makes

K_2CO_3 an excellent candidate for CO_2 capture at near-ambient temperatures. The practically achievable CO_2 uptake by K_2CO_3 is as high as 28.7 wt% (90.3 mol%).¹³⁸ However, the cyclic stability of K_2CO_3 is limited.

To improve the cyclic stability, researchers have impregnated K_2CO_3 on various types of high melting point supports. The most readily available support material is alumina.¹³⁹ However, the interaction between Al_2O_3 and K_2CO_3 would form the thermally stable $\text{KAl}(\text{CO}_3)(\text{OH})_2$:¹⁴⁰



which results in drastic capacity loss (9.6 wt%, to 4.8 wt%, *i.e.* 30.2 mol% to 15.1 mol%) after only 3 cycles.¹⁴¹ One way to avoid $\text{KAl}(\text{CO}_3)(\text{OH})_2$ formation is to restrict the operation to ambient temperatures and perform pressure swing cycles instead.¹⁴² However, the cost-benefit of doing pressure swing CO_2 capture must be further justified, as pressure swing processes are often associated with high energy penalties and additional costs arising from gas compression.

Alternatively, support materials that do not react with K_2CO_3 can be used, such as silicates (*e.g.* $\text{Al}_6\text{Si}_2\text{O}_{13}$, CaSiO_3 , ZrSiO_4 , which inert towards K_2CO_3),¹⁴¹ ZrO_2 (ref. 139) and porous carbon.¹⁴³ In all cases, stable performance over 10 cycles can be achieved at the expense of reduced CO_2 uptake (6.5–11.8 wt%, *i.e.* 20.4–37.1 mol% *cf.* the stoichiometric maximum of 31.8 wt%). Most interestingly, Yang *et al.*¹⁴³ impregnated K_2CO_3 on carbon aerogels, which possess extremely specific high surface areas (350 to 450 $\text{m}^2 \text{g}^{-1}$) and provide additional physisorption sites for CO_2 . As a result, they reported the highest CO_2 uptake of 9.2–11.8 wt% (28.9–37.1 mol%), amongst the highest of all supported K_2CO_3 sorbents. Nevertheless, the

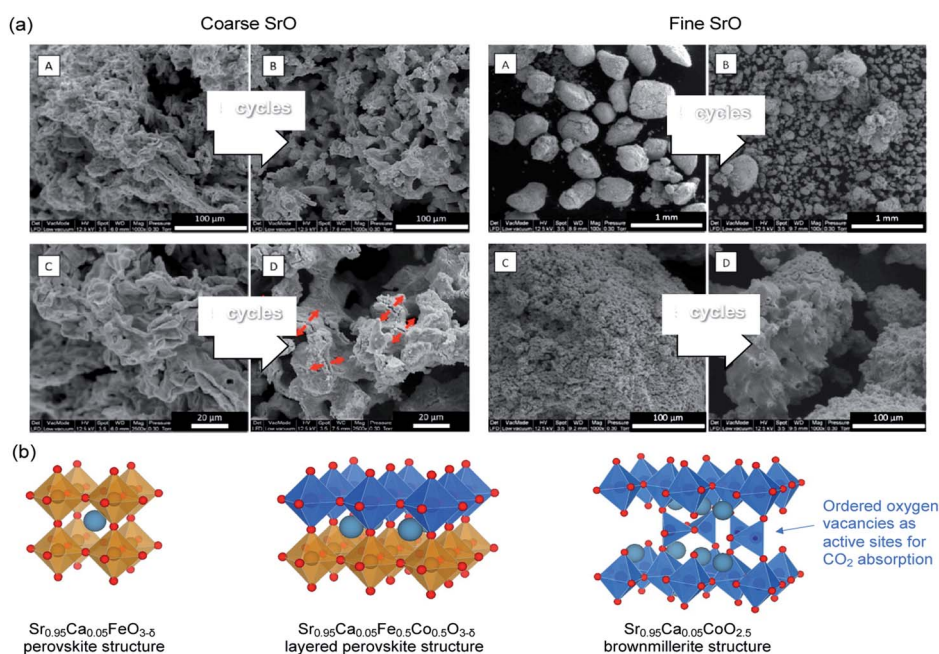


Fig. 14 (a) SEM images of coarse and fine SrO particles before (A & C) and after five cycles (B & D) of carbonation–calcination at 1100 °C (b) $\text{Sr}_{0.95}\text{Ca}_{0.05}\text{Fe}_{0.5}\text{Co}_{0.5}\text{O}_{3-\delta}$ perovskite with a layered structure and its phase segregation to a Fe-rich and a Co-rich phase. The undercoordinated Co sites are considered to be the preferential sites for CO_2 absorption. Reprinted with permission¹⁴⁴ copyright 2021 American Chemical Society.



application of the carbon based supports for CO₂ capture must be further validated under realistic operation conditions, considering the lack of CO₂ selectivity by the physisorption process and the lack of stability of carbon in the presence of oxygen, a common component in combustion flue gases.

4.4 Sr based sorbents

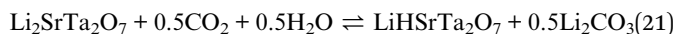
SrO can function by itself as a high temperature (>1000 °C) CO₂ sorbent with relatively high initial CO₂ uptake. Indeed, Miccio *et al.*¹⁴⁴ prepared SrO sorbents with mean particle size of 0.5 mm and 5.0 mm by calcining SrCO₃ and wet-granulation (Fig. 14a). The SrO sorbents with mean particle size of 0.5 mm and 5.0 mm had specific surface areas of 1.3 and 2.2 m² g⁻¹, respectively.¹⁴⁴ Both the fine, low surface area and coarse, high surface area SrO particles showed high initial CO₂ uptake capacities of 37.1 and 30.5 wt% (87.3 and 48.2 mol%), respectively, when tested in 50% CO₂ at 1100 °C. However, the uptake capacity rapidly dropped over cycles due to sintering. The attempt to support SrO₂ on Al₂O₃ by mechanical mixing resulted in the formation of Sr₃Al₂O₆ and SrAl₂O₄, both appeared beneficial to the sorbent's cyclic stability, at the expense of reducing the capture capacity to 8.7–9.3 wt% (20.5–21.9 mol%).

Alternatively, Sr-containing perovskites, in which Sr occupies the A sites in the ABO₃ lattice, can be used directly as CO₂ sorbents. These perovskite structured sorbents are typically prepared *via* sol-gel synthesis.¹⁴⁵ The A site and B site occupancies of the perovskites can be flexibly adjusted by varying the compositions of the metal precursors during the sol-gel synthesis. The site occupancies in turn influence the CO₂ capture performance. For example, La_{0.1}Sr_{0.9}Co_{0.5}Fe_{0.5}O_{3-δ} was found to capture more CO₂ (17.3 wt%, *i.e.* 83.6 mol%) than Sr_{0.95}Ca_{0.05}Fe_{0.5}Co_{0.5}O_{3-δ} (4.48 wt%, *i.e.* 18.3–33.2 mol%).^{146,147} However, further increasing the Ca occupancy in the A site (replacing more Sr) to Sr_{0.5}Ca_{0.5}Fe_{0.5}Co_{0.5}O_{3-δ} could improve the uptake to 17 wt% (62.3 mol%).¹⁴⁷ Such improvement was attributed to the fact that Sr_{0.5}Ca_{0.5}Fe_{0.5}Co_{0.5}O_{3-δ} with δ ≈ 0.53 corresponds to a brownmillerite structure (see Fig. 14b) with ordered oxygen vacancies, which are regarded by many to be beneficial to CO₂ uptake:^{146,148}



Adjusting the B-site occupancies could also influence the capture performance. Lu *et al.*¹⁴⁹ synthesised SrCo_{1-2x}(Fe, Nb)_xO_{3-δ} with equimolar amount of Fe and Nb by solid-state reactions between SrCO₃, Co₃O₄ (or Co₂O₃), Fe₂O₃, and Nb₂O₅. For x = 0.05 and 0.10, the freshly synthesised sorbents showed CO₂ uptake of 13.1 wt% (55.5 mol%) and 11.1 wt% (47.0 mol%), respectively, when evaluated in 75% CO₂ at 925 °C. Here, the increased B site occupancy by Nb enhanced the acidity and reduced the activity of the perovskite towards carbonation.¹⁵⁰

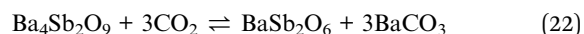
Beyond the cubic-perovskite structure, a Ruddlesden-Popper (RP) structured (A'₂[A_{n-1}B_nO_{3n+1}]) Li₂SrTa₂O₇ sorbent was prepared by Galven *et al.* by solid state synthesis.¹⁵¹ This RP phase achieved 4.90 wt% (96.1 mol%) uptake (with a stoichiometric uptake of 5.11 wt%) after 15 h in humid CO₂ at 140 °C, 30 bar pressure:



In addition, the Li₂SrTa₂O₇ sorbent exhibited excellent cyclability with negligible capacity loss over 6 cycles of isothermal carbonation at 140 °C and regeneration up to 700 °C. Such performance merits further development and investigation.

4.5 Ba based sorbents

Like Sr based sorbents, most studies on Ba based sorbents focus on the use of perovskite-type oxides with Ba occupying the A sites. These Ba based perovskites can be prepared by either sol-gel synthesis¹⁴⁸ or solid state reactions.¹⁵² Likewise, the performance of the Ba based sorbents also depends on the site occupancies. For example, Nomura *et al.*¹⁴⁸ found that changing the Fe occupancy in (Ba_{0.95}Ca_{0.05})(Co_{1-x}Fe_x)O_{3-δ} from 0.2 to 0.9 resulted in a reduction in CO₂ uptake from 10.0 wt% (52.5 mol%) to 8.7 wt% (45.3 mol%). Given that BaFeO_{3-δ} (0 < δ < 0.5) type materials are capable of reversibly changing phase between perovskite (ABO₃) and brownmillerite (A₂B₂O₅), facilitated by oxygen uptake and release, their CO₂ capture performance would also dependent on the oxygen partial pressure and the temperature. In general, unstable BaFeO_{3-δ} structures correspond to improved CO₂ capture performance. For example, carbonating Ba_{0.95}Ca_{0.05}Co_{0.8}Fe_{0.2}O_{3-δ} in the absence of oxygen renders an improved capture capacity of 12 wt% (62.5 mol%), owing to the thermal decomposition of perovskite to brownmillerite, which appeared as a better sorbent; this finding is in agreement with Lu *et al.*¹⁴⁹ and Fujishiro *et al.*¹⁵³ Yi *et al.* doped the B-sites of BaFeO_{3-δ} with Nb,¹⁵⁴ and reported low CO₂ uptake (1.3 wt%, 6.9 mol%) of the doped perovskite. We suspect that the Nb dopant donates electrons to the perovskite structure, which becomes chemically stabilised and unreactive towards CO₂. The most outstanding Ba based sorbents is perhaps the 6H-perovskite Ba₄Sb₂O₉ reported by Dunstan *et al.*¹⁵⁵ The authors prepared the sorbents by solid-state reaction between BaCO₃ and Sb₂O₃. Ba₄Sb₂O₉ reacts with CO₂ with a stoichiometric CO₂ uptake capacity of 14.1 wt%:



Experimentally, near-stoichiometric CO₂ uptake of 13.75 wt% (99.3 mol%) was observed upon carbonation at 750 °C. During long-term cyclic operation, Ba₄Sb₂O₉ showed >10 wt% (70.9 mol%) CO₂ uptake over 100 uptake-regeneration cycles (Fig. 15a). The excellent cyclic stability of Ba₄Sb₂O₉ originated from the sorbent's ability to fully regenerate its complete pore structure in each cycle, despite the fact that the fully carbonated sorbent showed virtually no porosity (Fig. 15b). The same authors also found Ba₄Nb_{2-x}Ta_xO₉ materials to be poor CO₂ sorbents, showing uptake <0.07 wt% in 100% CO₂ at up to 1000 °C.¹⁵⁶

4.6 Summary and knowledge gap

Compared to the CaO and MgO based sorbents, Li, Na, K, Sr and Ba based sorbents are less commonly studied. Owing to the



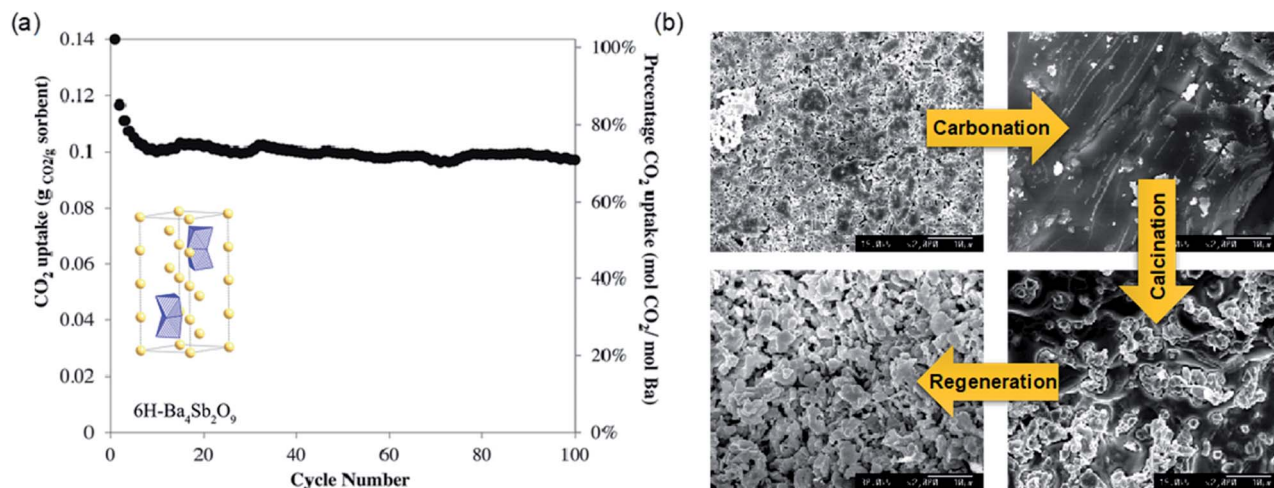


Fig. 15 (a) CO₂ uptake by 6H perovskite Ba₄Sb₂O₉ over 100 carbonation–calcination cycles in at TGA. (b) Surface morphology Ba₄Sb₂O₉ as it evolves over carbonation–calcination cycles. Reprinted with permission¹⁵⁵ copyright 2021 American Chemical Society.

high alkalinity of the metal sites, Li, Na, K, Sr and Ba based oxides require chemical modifications to function as reversible CO₂ sorbents at reasonable temperatures. These chemical modifications refer to a large pool of candidate sorbent compositions. Whilst many of these sorbents behave similarly during CO₂ uptake (*e.g.*, the double shell model for lithium silicates, lithium zirconates, sodium silicates and sodium zirconates), significantly more research is needed to fully understand and rationalise the behaviour of these mixed oxide sorbents in relation to their chemical composition, structure and synthesis methods. Following the discussion above, we summarise the following knowledge gaps for Li, Na, K, Sr and Ba based sorbents:

- The effect of strain development on the product layers during carbonation (*e.g.* following the double shell model depicted in Fig. 12a) is not well understood.
- Most of the sorbents discussed in this section have not been tested under practical CO₂ capture conditions, *i.e.* carbonation in 5–15% CO₂ (in the presence of moisture) and calcination in pure CO₂.
- The test conditions employed by different studies are inconsistent, making it difficult to make fair comparisons.
- Most CO₂ uptake tests were done in TGA, whilst some sorbents have only been studied for 1 carbonation cycle or by temperature programme carbonation.
- The synthesis parameters have not been sufficiently explored to identify optimal synthesis procedures.
- The cost-benefit of synthesising sorbents with complex structures and compositions must be justified.

5 Challenges and opportunities

This review discusses the recent advances in developing synthetic oxide sorbents for CO₂ capture. The CO₂ uptake ability of these sorbents originates from the alkalinity of the group 1 and group 2 metals. Because of reasons associated with cost, natural abundance and the performance of the natural mineral-

derived sorbents, different classes of solid oxide sorbents have received varying extents of research attention and have reached different levels of technological maturity. Specifically, CaO based sorbents can be produced at large quantities from low-cost Ca sources (*e.g.* limestone), and have been extensively tested over a wide range of scales (from TGA to pilot plants) in realistic flue gas compositions. In contrast, all non-CaO based sorbents require specific chemical modifications to achieve improved CO₂ capture kinetics and capacity. Furthermore, the lack of testing standards for the non-CaO sorbents makes it difficult to have meaningful comparisons between different studies, even if they report similar chemical formulations. Addressing the lack of testing standards with priority will allow the field to develop faster and more efficiently.

There is also much commonality between different classes of sorbents. For instance, the carbonation of almost all solid oxide sorbents depends on the porosity and the mass transfer through the carbonated product layer. However, maintaining the porous structure of a solid material while it undergoes many cycles of phase changes (*i.e.* between oxides and carbonates) is technically challenging. Indeed, much research has been devoted to improving the cyclic stability of the solid oxide sorbents through synthetic approaches. One of the key methods involves mixing the active sorbent phases with thermal stabilisers such as Al₂O₃ and ZrO₂. Here, the chemical interaction between the active component (solid bases) and the thermal stabilizer phases (typically acidic oxides) must be understood and taken into consideration, as these interactions could potentially form inert phases (*e.g.* Ca₁₂Al₁₄O₃₃ and KAl(CO₃)(OH)₂) to dilute the CO₂ uptake capacity of the composite sorbents.

The synthetic approaches to improve the CO₂ uptake kinetics are also equally applicable across different classes of sorbents. For example, doping the sorbent surface with low-melting point salts could result in the formation of a molten salt layer during high temperature operation. Consequently, the mass transfer of CO₂ through the carbonate product layer can be drastically improved. Doping redox active metals such as Fe³⁺ could further



enhance the mass transfer, which is governed by ionic diffusion through the molten layer, thereby achieving fast CO₂ capture and high CO₂ uptake capacity. For sorbents that do not rely on the functioning of the molten salt layer, it is generally beneficial to prepare sorbents with high specific surface area and high porosity. To this end, the knowledge in preparing CaO based sorbents, *e.g.* the effect of synthesis parameters on the morphological properties of the final products, can be adapted for improving the performance of other types of oxide sorbents for a wide range of process applications.

For applications where the capturing and regeneration should take place at moderate to low temperatures, there is also an opportunity to hybridise metal oxides with membranes, polymers, and carbon-based materials to yield synergistic effects and enhanced sorbent performance.^{157–159} For instance, it has been reported that doping membranes with metal oxides resulted in improved CO₂ uptake. Doped membranes with polar –OH group on the surfaces can increase the membrane sorbent's reactivity with CO₂ molecules – as CO₂ molecules and metal oxide act as electron acceptors and donors, respectively, the selectivity and permeability of the oxide-doped membrane towards CO₂ molecules can be effectively increased.^{160–162} On the other hand, more research effort is required to improve the cyclic regenerability and durability of these composite sorbent materials.

Beyond experimental approaches, the emerging of computational chemistry has offered opportunity to accelerate sorbent formulation with unprecedented efficiencies. In fact, computational approaches have been widely adopted by chemists developing solid sorbents based on MOFs, zeolites and carbon materials,^{163–166} including high-throughput screening studies that explored candidate sorbent materials in computational databases.^{167–170} For solid oxide sorbents, *ab initio* computational studies would in the first instance rely on density functional theory (DFT) calculations to predict the properties of the oxides and the active sites for CO₂ uptake. Dunstan *et al.* has conducted a pioneering high throughput screening of oxidic CO₂ sorbent materials using the Materials Project database and identified Na₃SbO₄ and Li₅FeO₄ to be promising CO₂ sorbents.¹⁹ Similarly, the computational screening by Gaultois *et al.* found Li₅SbO₅ as a potential sorbent, which showed satisfactory CO₂ uptake performance (~72% of its stoichiometric uptake capacity) over 25 cycles.¹³⁰ At present, there remains a gap between the thermochemical material properties that are computationally predicted and those experimentally measured. Such gap could potentially hinder the effective of the computational approaches to discover and develop new sorbents. However, with the rapid advancement in computational methods to simulate detailed chemical and physical phenomena, we anticipate computer-aided materials design methods to play major roles in the future development of solid oxide CO₂ sorbents.

Author contributions

Ribooga Chang: data curation, formal analysis, writing – original draft, writing – review & editing; Xianyu Wu: data curation,

formal analysis, writing – original draft, writing – review & editing; Ocean Cheung: conceptualization, funding acquisition, supervision, writing – review & editing; Wen Liu: conceptualization, funding acquisition, supervision, writing – review & editing.

Conflicts of interest

There are no conflicts to declare.

Acknowledgements

R. C. and O. C. thank the Swedish Foundation for International Cooperation in Research and Higher Education (STINT) (Grant no. IB2019-8184), the Swedish Research Council (Grant no. 2020-04029) and Swedish Research Council for Sustainable Development (FORMAS, Grant no. 2018-00651) for their financial support. W. L. acknowledges the financial support by National Research Foundation of Singapore under its Campus of Research Excellence and Technological Enterprise (CRETE) programme.

References

- 1 M. Z. Akram, V. Atla, A. Nambo, B. P. Ajayi, J. B. Jasinski, J. He, J. R. Gong and M. Sunkara, *Nano Lett.*, 2018, **18**, 4891–4899.
- 2 G. D. Farquhar, M. L. Goulden, M. J. R. Fasham, M. Heimann, V. J. Jaramillo, H. S. Khesghi, C. Le Quéré, R. J. Scholes and D. W. R. Wallace, *IPCC*, 2001.
- 3 M. Bui, C. S. Adjiman, A. Bardow, E. J. Anthony, A. Boston, S. Brown, P. S. Fennell, S. Fuss, A. Galindo, L. A. Hackett, J. P. Hallett, H. J. Herzog, G. Jackson, J. Kemper, S. Krevor, G. C. Maitland, M. Matuszewski, I. S. Metcalfe, C. Petit, G. Puxty, J. Reimer, D. M. Reiner, E. S. Rubin, S. A. Scott, N. Shah, B. Smit, J. P. M. Trusler, P. Webley, J. Wilcox and N. Mac Dowell, *Energy Environ. Sci.*, 2018, **11**, 1062–1176.
- 4 R. Stanger, T. Wall, R. Spörl, M. Paneru, S. Grathwohl, M. Weidmann, G. Scheffknecht, D. McDonald, K. Myöhänen, J. Ritvanen, S. Rahiala, T. Hyppänen, J. Mletzko, A. Kather and S. Santos, *Int. J. Greenhouse Gas Control*, 2015, **40**, 55–125.
- 5 M. Finkenrath, *Chem. Eng. Technol.*, 2012, **35**, 482–488.
- 6 A. Brunetti, F. Scura, G. Barbieri and E. Drioli, *J. Membr. Sci.*, 2010, **359**, 115–125.
- 7 F. Vega, A. Sanna, B. Navarrete, M. M. Maroto-Valer and V. J. Cortés, *Greenhouse Gases: Sci. Technol.*, 2014, **4**, 707–733.
- 8 S. Kumar, R. Srivastava and J. Koh, *J. CO₂ Util.*, 2020, **41**, 101251.
- 9 Z. Hu, Y. Wang, B. B. Shah and D. Zhao, *Adv. Sustainable Syst.*, 2019, **3**, 1800080.
- 10 O. Cheung and N. Hedin, *RSC Adv.*, 2014, **4**, 14480–14494.
- 11 M. Ding, R. W. Flaig, H.-L. Jiang and O. M. Yaghi, *Chem. Soc. Rev.*, 2019, **48**, 2783–2828.



- 12 O. K. Farha, A. Özgür Yazaydın, I. Eryazici, C. D. Malliakas, B. G. Hauser, M. G. Kanatzidis, S. T. Nguyen, R. Q. Snurr and J. T. Hupp, *Nat. Chem.*, 2010, **2**, 944–948.
- 13 L. H. Xie, M. M. Xu, X. M. Liu, M. J. Zhao and J. R. Li, *Adv. Sci.*, 2020, **7**, 1901758.
- 14 S. Mukherjee, S. Sharma and S. K. Ghosh, *APL Mater.*, 2019, **7**, 050701.
- 15 N. Ghasem, in *Advances in Carbon Capture*, 2020, pp. 479–501.
- 16 C. Song, Q. Liu, S. Deng, H. Li and Y. Kitamura, *Renewable Sustainable Energy Rev.*, 2019, **101**, 265–278.
- 17 G. Ji and M. Zhao, *Recent Advances in Carbon Capture and Storage*, 2017, ch. 3, DOI: DOI: 10.5772/65723.
- 18 U. W. R. Siagian, A. Raksajati, N. F. Himma, K. Khoiruddin and I. G. Wenten, *J. Nat. Gas Sci. Eng.*, 2019, **67**, 172–195.
- 19 M. T. Dunstan, A. Jain, W. Liu, S. P. Ong, T. Liu, J. Lee, K. A. Persson, S. A. Scott, J. S. Dennis and C. P. Grey, *Energy Environ. Sci.*, 2016, **9**, 1346–1360.
- 20 J. Blamey, E. J. Anthony, J. Wang and P. S. Fennell, *Prog. Energy Combust. Sci.*, 2010, **36**, 260–279.
- 21 C. C. Dean, J. Blamey, N. H. Florin, M. J. Al-Jeboori and P. S. Fennell, *Chem. Eng. Res. Des.*, 2011, **89**, 836–855.
- 22 M. Reitz, M. Junk, J. Ströhle and B. Eppele, *Int. J. Greenhouse Gas Control*, 2016, **54**, 272–281.
- 23 J. A. Duffy, *J. Am. Ceram. Soc.*, 1997, **80**, 1416–1420.
- 24 J. A. Duffy, *Geochim. Cosmochim. Acta*, 1993, **57**, 3961–3970.
- 25 J. Wang, L. Huang, R. Yang, Z. Zhang, J. Wu, Y. Gao, Q. Wang, D. O'Hare and Z. Zhong, *Energy Environ. Sci.*, 2014, **7**, 3478–3518.
- 26 M. T. Dunstan, F. Donat, A. H. Bork, C. P. Grey and C. R. Müller, *Chem. Rev.*, 2021, **121**, 12681–12745.
- 27 A. Perejón, L. M. Romeo, Y. Lara, P. Lisbona, A. Martínez and J. M. Valverde, *Appl. Energy*, 2016, **162**, 787–807.
- 28 M. C. Romano, I. Martínez, R. Murillo, B. Arstad, R. Blom, D. C. Ozcan, H. Ahn and S. Brandani, *Energy Procedia*, 2013, **37**, 142–150.
- 29 A. M. Kierzkowska, R. Pacciani and C. R. Muller, *J. Mater. Chem. A*, 2013, **6**, 1130–1148.
- 30 T. Xu, X. Wang, B. Xiao and W. Liu, *Chem. Eng. J.*, 2021, **425**, 131522.
- 31 IEA, *The challenge of reaching zero emissions in heavy industry*, IEA, Paris, 2020, <https://www.iea.org/articles/the-challenge-of-reaching-zero-emissions-in-heavy-industry>.
- 32 S. Gardarsdottir, E. De Lena, M. Romano, S. Roussanaly, M. Voldsund, J.-F. Pérez-Calvo, D. Berstad, C. Fu, R. Anantharaman, D. Sutter, M. Gazzani, M. Mazzotti and G. Cinti, *Energies*, 2019, **12**, 542.
- 33 M. C. Romano, M. Spinelli, S. Campanari, S. Consonni, G. Cinti, M. Marchi and E. Borgarello, *Energy Procedia*, 2013, **37**, 7091–7099.
- 34 B. Arias, M. E. Diego, J. C. Abanades, M. Lorenzo, L. Diaz, D. Martínez, J. Alvarez and A. Sánchez-Biezma, *Int. J. Greenhouse Gas Control*, 2013, **18**, 237–245.
- 35 M.-H. Chang, W.-C. Chen, C.-M. Huang, W.-H. Liu, Y.-C. Chou, W.-C. Chang, W. Chen, J.-Y. Cheng, K.-E. Huang and H.-W. Hsu, *Energy Procedia*, 2014, **63**, 2100–2108.
- 36 B. Arias, M. Alonso and C. Abanades, *Ind. Eng. Chem. Res.*, 2017, **56**, 2634–2640.
- 37 M. Erans, M. Jeremias, V. Manovic and E. J. Anthony, *J. Visualized Exp.*, 2017, **128**, e56122.
- 38 A. de la Calle Martos, J. M. Valverde, P. E. Sanchez-Jimenez, A. Perejon, C. Garcia-Garrido and L. A. Perez-Maqueda, *Phys. Chem. Chem. Phys.*, 2016, **18**, 16325–16336.
- 39 C. Zhongxiang, H. S. Song, M. Portillo, C. J. Lim, J. R. Grace and E. J. Anthony, *Energy Fuels*, 2009, **23**, 1437–1444.
- 40 H. Sun, C. Wu, B. Shen, X. Zhang, Y. Zhang and J. Huang, *Mater. Today Sustain.*, 2018, **1–2**, 1–27.
- 41 Y. Hu, H. Lu, W. Liu, Y. Yang and H. Li, *Chem. Eng. J.*, 2020, **396**, 125253.
- 42 J. M. Valverde, *J. Nanopart. Res.*, 2018, **20**, 39.
- 43 V. Manovic and E. J. Anthony, *Ind. Eng. Chem. Res.*, 2010, **49**, 9105–9110.
- 44 S. Yang and Y. Xiao, *Ind. Eng. Chem. Res.*, 2008, **47**, 4043–4048.
- 45 J. Yin, C. Zhang, C. Qin, W. Liu, H. An, G. Chen and B. Feng, *Chem. Eng. J.*, 2012, **198–199**, 38–44.
- 46 B. Arias, G. S. Grasa and J. C. Abanades, *Chem. Eng. J.*, 2010, **163**, 324–330.
- 47 A. N. Antzara, A. Arregi, E. Heracleous and A. A. Lemonidou, *Chem. Eng. J.*, 2018, **333**, 697.
- 48 H. Guo, S. Yan, Y. Zhao, X. Ma and S. Wang, *Chem. Eng. J.*, 2019, **359**, 542–551.
- 49 J. Sun, W. Wang, Y. Yang, S. Cheng, Y. Guo, C. Zhao, W. Liu and P. Lu, *Fuel*, 2020, **266**, 117056.
- 50 V. Manovic and E. J. Anthony, *Environ. Sci. Technol.*, 2008, **42**, 4170–4174.
- 51 K. Labus, *Materials*, 2021, **14**, 548.
- 52 A. H. Soleimanisalim, M. H. Sedghkardar, D. Karami and N. Mahinpey, *J. Nat. Gas Sci. Eng.*, 2016, **36**, 1056–1061.
- 53 S. M. Hashemi, D. Karami and N. Mahinpey, *Fuel*, 2020, **269**, 117432.
- 54 A. Kurlov, A. Armutlulu, F. Donat, A. R. Studart and C. R. Müller, *Ind. Eng. Chem. Res.*, 2019, **59**, 7182–7188.
- 55 H. Sun, J. Wang, J. Zhao, B. Shen, J. Shi, J. Huang and C. Wu, *Appl. Catal., B*, 2019, **244**, 63–75.
- 56 M. Vall, J. Hultberg, M. Strømme and O. Cheung, *RSC Adv.*, 2019, **9**, 20273–20280.
- 57 C. Luo, Y. Zheng, N. Ding, Q. L. Wu and C. G. Zheng, *Chin. Chem. Lett.*, 2011, **22**, 615–618.
- 58 H. J. Yoon and K. B. Lee, *Chem. Eng. J.*, 2019, **355**, 850–857.
- 59 K. S. Sultana, D. T. Tran, J. C. Walmsley, M. Rønning and D. Chen, *Ind. Eng. Chem. Res.*, 2015, **54**, 8929–8939.
- 60 N. Gao, K. Chen and C. Quan, *Fuel*, 2020, **260**, 116411.
- 61 R. Han, J. Gao, S. Wei, Y. Su and Y. Qin, *J. Mater. Chem. A*, 2018, **6**, 3462–3470.
- 62 A. Armutlulu, M. A. Naeem, H. J. Liu, S. M. Kim, A. Kierzkowska, A. Fedorov and C. R. Muller, *Adv. Mater.*, 2017, **29**, 1702896.
- 63 W. Peng, Z. Xu, C. Luo and H. Zhao, *Environ. Sci. Technol.*, 2015, **49**, 8237–8245.
- 64 W. Liu, H. An, C. Qin, J. Yin, G. Wang, B. Feng and M. Xu, *Energy Fuels*, 2012, **26**, 2751–2767.



- 65 B. Azimi, M. Tahmasebpour, P. E. Sanchez-Jimenez, A. Perejon and J. M. Valverde, *Chem. Eng. J.*, 2019, **358**, 679–690.
- 66 X. Kou, C. Li, Y. Zhao, S. Wang and X. Ma, *Fuel Process. Technol.*, 2018, **177**, 210–218.
- 67 Y. Wang, W. Zhang, R. Li, W. Duan and B. Liu, *Energy Fuels*, 2016, 1248–1255.
- 68 A. N. Antzara, A. Arregi, E. Heracleous and A. A. Lemonidou, *Chem. Eng. J.*, 2018, **333**, 697–711.
- 69 H. Ping and S. Wu, *RSC Adv.*, 2015, **5**, 65052–65057.
- 70 S. Wang, H. Shen, S. Fan, Y. Zhao, X. Ma and J. Gong, *Chem. Eng. Sci.*, 2015, **135**, 532–539.
- 71 M. A. Naeem, A. Armutlulu, Q. Imtiaz and C. R. Müller, *ChemPhysChem*, 2017, **18**, 3280.
- 72 P. Jamrunroj, S. Wongsakulphasatch, A. Maneedaeng, C. K. Cheng and S. Assabumrungrat, *Powder Technol.*, 2019, **344**, 208–221.
- 73 J. Chen, T. Shi, L. Duan, Z. Sun and E. J. Anthony, *Chem. Eng. J.*, 2020, **393**, 124716.
- 74 C. Qin, W. Liu, H. An, J. Yin and B. Feng, *Environ. Sci. Technol.*, 2012, **46**, 1932–1939.
- 75 Z. Zhou, Y. Qi, M. Xie, Z. Cheng and W. Yuan, *Chem. Eng. Sci.*, 2012, **74**, 172–180.
- 76 C.-H. Huang, K.-P. Chang, C.-T. Yu, P.-C. Chiang and C.-F. Wang, *Chem. Eng. J.*, 2010, **161**, 129–135.
- 77 M. Olivares-Marin, E. M. Cuerda-Correa, A. Nieto-Sánchez, S. García, C. Pevida and S. Román, *Chem. Eng. J.*, 2013, **217**, 71–81.
- 78 M. Broda and C. R. Müller, *Fuel*, 2014, **127**, 94–100.
- 79 X. Yan, Y. Li, X. Ma, J. Zhao, Z. Wang and H. Liu, *New J. Chem.*, 2019, **43**, 5116–5125.
- 80 L. Huang, Q. Zheng, B. Louis and Q. Wang, *Energy Technol.*, 2018, **6**, 2469–2478.
- 81 S. Wei, R. Han, Y. Su, J. Gao, G. Zhao and Y. Qin, *Energy Fuels*, 2019, **33**, 5398–5407.
- 82 Y. Hu, Y. Guo, J. Sun, H. Li and W. Liu, *J. Mater. Chem. A*, 2019, **7**, 20103–20120.
- 83 B. W. Hwang, J. H. Lim, H. J. Chae, H.-J. Ryu, D. Lee, J. B. Lee, H. Kim, S. C. Lee and J. C. Kim, *Process Saf. Environ. Prot.*, 2018, **116**, 219–227.
- 84 X. Zhao, G. Ji, W. Liu, X. He, E. J. Anthony and M. Zhao, *Chem. Eng. J.*, 2018, **332**, 216–226.
- 85 A. Dal Pozzo, A. Armutlulu, M. Rekhtina, P. M. Abdala and C. R. Müller, *ACS Appl. Energy Mater.*, 2019, **2**, 1295–1307.
- 86 T. Harada and T. A. Hatton, *Chem. Mater.*, 2015, **27**, 8153–8161.
- 87 J. S. Kwak, K. R. Oh, K. Y. Kim, J. M. Lee and Y. U. Kwon, *Phys. Chem. Chem. Phys.*, 2019, **21**, 20805–20813.
- 88 J. Ding, C. Yu, J. Lu, X. Wei, W. Wang and G. Pan, *Appl. Energy*, 2020, **263**, 114681.
- 89 S. Jin, K. Ho and C.-H. Lee, *Chem. Eng. J.*, 2018, **334**, 1605–1613.
- 90 H. Joo, S. J. Cho and K. Na, *J. CO₂ Util.*, 2017, **19**, 194–201.
- 91 A.-T. Vu, K. Ho, S. Jin and C.-H. Lee, *Chem. Eng. J.*, 2016, **291**, 161–173.
- 92 L. Wang, Z. Zhou, Y. Hu, Z. Cheng and X. Fang, *Ind. Eng. Chem. Res.*, 2017, **56**, 5802–5812.
- 93 Y. Yoo, D. Kang, E. Choi, J. Park and I.-S. Huh, *Chem. Eng. J.*, 2019, **370**, 237–250.
- 94 Y. Guo, C. Tan, P. Wang, J. Sun, W. Li, C. Zhao and P. Lu, *Chem. Eng. J.*, 2020, **379**, 122277.
- 95 Y.-D. Ding, G. Song, X. Zhu, R. Chen and Q. Liao, *RSC Adv.*, 2015, **5**, 30929–30935.
- 96 A. Hanif, S. Dasgupta and A. Nanoti, *Ind. Eng. Chem. Res.*, 2016, **55**, 8070–8078.
- 97 V. A. Tuan and C. H. Lee, *Vietnam J. Chem.*, 2018, **56**, 197–202.
- 98 P. Li, W. Liu, J. S. Dennis and H. C. Zeng, *ACS Appl. Mater. Interfaces*, 2017, **9**, 9592–9602.
- 99 P. Li, Y. Lin, R. Chen and W. Li, *Dalton Trans.*, 2020, **49**, 5183–5191.
- 100 P. Li and H. C. Zeng, *Environ. Sci. Technol.*, 2017, **51**, 12998–13007.
- 101 H.-H. Lee, J.-C. Lee, Y.-J. Joo, M. Oh and C.-H. Lee, *Appl. Energy*, 2014, **131**, 425–440.
- 102 H. Cui, Q. Zhang, Y. Hu, C. Peng, X. Fang, Z. Cheng, V. V. Galvita and Z. Zhou, *ACS Appl. Mater. Interfaces*, 2018, **10**, 20611–20620.
- 103 A. H. Bork, M. Rekhtina, E. Willinger, P. Castro-Fernández, J. Drnec, P. M. Abdala and C. R. Müller, *Proc. Natl. Acad. Sci.*, 2021, **118**, e2103971118.
- 104 G. Xiao, R. Singh, A. Chaffee and P. Webley, *Int. J. Greenhouse Gas Control*, 2011, **5**, 634–639.
- 105 A.-T. Vu, Y. Park, P. R. Jeon and C.-H. Lee, *Chem. Eng. J.*, 2014, **258**, 254–264.
- 106 C. H. Lee, S. Mun and K. B. Lee, *Chem. Eng. J.*, 2014, **258**, 367–373.
- 107 K. Zhang, X. S. Li, Y. Duan, D. L. King, P. Singh and L. Li, *Int. J. Greenhouse Gas Control*, 2013, **12**, 351–358.
- 108 S. I. Jo, Y. I. An, K. Y. Kim, S. Y. Choi, J. S. Kwak, K. R. Oh and Y. U. Kwon, *Phys. Chem. Chem. Phys.*, 2017, **19**, 6224–6232.
- 109 Y. Qiao, J. Wang, Y. Zhang, W. Gao, T. Harada, L. Huang, T. A. Hatton and Q. Wang, *Ind. Eng. Chem. Res.*, 2017, **56**, 1509–1517.
- 110 Q. Wang, H. H. Tay, Z. Guo, L. Chen, Y. Liu, J. Chang, Z. Zhong, J. Luo and A. Borgna, *Appl. Clay Sci.*, 2012, **55**, 18–26.
- 111 M. L. T. Trivino, V. Hiremath and J. G. Seo, *Environ. Sci. Technol.*, 2018, **52**, 11952–11959.
- 112 S. Jin, K.-J. Ko and C.-H. Lee, *Chem. Eng. J.*, 2019, **371**, 64–77.
- 113 K. K. Han, Y. Zhou, Y. Chun and J. H. Zhu, *J. Hazard. Mater.*, 2012, **203–204**, 341–347.
- 114 X. Yang, W. Liu, J. Sun, Y. Hu, W. Wang, H. Chen, Y. Zhang, X. Li and M. Xu, *ChemSusChem*, 2016, **9**, 1607–1613.
- 115 F. Cova, G. Amica, K. Kohopää and M. V. Blanco, *Inorg. Chem.*, 2019, **58**, 1040–1047.
- 116 H. Wang, J. Zhang, G. Wang, Q. Wang and T. Song, *J. Therm. Anal. Calorim.*, 2018, **133**, 981–989.
- 117 X. Chen, Z. Xiong, Y. Qin, B. Gong, C. Tian, Y. Zhao, J. Zhang and C. Zheng, *Int. J. Hydrogen Energy*, 2016, **41**, 13077–13085.



- 118 H. A. Lara-García, O. Ovalle-Encinia, J. Ortiz-Landeros, E. Lima and H. Pfeiffer, *J. Mater. Chem. A*, 2019, **7**, 4153–4164.
- 119 K. Wang, J. Hong, Z. Zhou, Z. Lin and P. Zhao, *Energy Technol.*, 2019, **7**, 325–332.
- 120 X. Yang, W. Liu, J. Sun, Y. Hu, W. Wang, H. Chen, Y. Zhang, X. Li and M. Xu, *ChemSusChem*, 2016, **9**, 2480–2487.
- 121 M. Seggiani, E. Stefanelli, M. Puccini and S. Vitolo, *Chem. Eng. J.*, 2018, **339**, 51–60.
- 122 N. Gómez-Garduño and H. Pfeiffer, *Thermochim. Acta*, 2019, **673**, 129–137.
- 123 D. Peltzer, J. Múnera, L. Cornaglia and M. Strumendo, *Chem. Eng. J.*, 2018, **336**, 1–11.
- 124 D. Peltzer, J. Múnera and L. Cornaglia, *J. Environ. Chem. Eng.*, 2019, **7**, 102927.
- 125 N. Togashi, T. Okumura and K. Oh-Ishi, *J. Ceram. Soc. Jpn.*, 2007, **115**, 324–328.
- 126 M. V. Blanco, K. Kohopää, I. Snigireva and F. Cova, *Chem. Eng. J.*, 2018, **354**, 370–377.
- 127 E. Bernabé-Pablo, F. Plascencia-Hernández, A. Yañez-Aulestia and H. Pfeiffer, *Chem. Eng. J.*, 2020, **384**, 123291.
- 128 M. A. Martínez-Cruz, A. Yañez-Aulestia, G. Ramos-Sánchez, M. Oliver-Tolentino, M. Vera, H. Pfeiffer, D. Ramírez-Rosales and I. González, *Dalton Trans.*, 2020, **49**, 4549–4558.
- 129 A. Yañez-Aulestia, Q. Wang and H. Pfeiffer, *Phys. Chem. Chem. Phys.*, 2020, **22**, 2803–2813.
- 130 M. W. Gaultois, M. T. Dunstan, A. W. Bateson, M. S. C. Chan and C. P. Grey, *Chem. Mater.*, 2018, **30**, 2535–2543.
- 131 T. Harada and T. A. Hatton, *J. Mater. Chem. A*, 2017, **5**, 22224–22233.
- 132 E. Vera, S. García, M. M. Maroto-Valer and H. Pfeiffer, *Adsorption*, 2020, **26**, 781–792.
- 133 J. Liu, Z. Wang, Z. Wang, J. Song, G. Li, Q. Xu, J. You, H. Cheng and X. Lu, *Phys. Chem. Chem. Phys.*, 2019, **21**, 13135–13143.
- 134 L. Martínez-dlCruz and H. Pfeiffer, *J. Phys. Chem. C*, 2012, **116**, 9675–9680.
- 135 G. Ji, M. Z. Memon, H. Zhuo and M. Zhao, *Chem. Eng. J.*, 2017, **313**, 646–654.
- 136 T. Zhao, E. Ochoa-Fernández, M. Rønning and D. Chen, *Chem. Mater.*, 2007, **19**, 3294–3301.
- 137 S. Munro, M. Åhlén, O. Cheung and A. Sanna, *Chem. Eng. J.*, 2020, **388**, 124284.
- 138 C. Zhao, X. Chen and C. Zhao, *Int. J. Greenhouse Gas Control*, 2010, **4**, 655–658.
- 139 S. C. Lee, H. J. Chae, S. J. Lee, Y. H. Park, C. K. Ryu, C. K. Yi and J. C. Kim, *J. Mol. Catal. B: Enzym.*, 2009, **56**, 179–184.
- 140 S. C. Lee and J. C. Kim, *Catal. Surv. Asia*, 2007, **11**, 171–185.
- 141 M. S. Cho, S. C. Lee, H. J. Chae, Y. M. Kwon, J. B. Lee and J. C. Kim, *Process Saf. Environ. Prot.*, 2018, **117**, 296–306.
- 142 S. Boonprasop, B. Chalermisinsuwan and P. Piumsomboon, *J. Taiwan Inst. Chem. Eng.*, 2018, **88**, 215–225.
- 143 G. Yang, H. Luo, T. Ohba and H. Kanoh, *Int. J. Chem. Eng.*, 2016, **2016**, 4012967.
- 144 F. Miccio, A. N. Murri and E. Landi, *Ind. Eng. Chem. Res.*, 2016, **55**, 6696–6707.
- 145 Q. Yang and Y. S. Lin, *Ind. Eng. Chem. Res.*, 2006, **45**, 6302–6310.
- 146 Z. Homonnay, K. Nomura, G. Juhász, M. Gál, K. Sólmos, S. Hamakawa, T. Hayakawa and A. Vértés, *Chem. Mater.*, 2002, **14**, 1127–1135.
- 147 G. Juhász, Z. o. Homonnay, K. Nomura, T. Hayakawa, S. Hamakawa and A. Vértés, *Solid State Ionics*, 2001, **139**, 219–231.
- 148 K. Nomura, Y. Ujihira, T. Hayakawa and K. Takehira, *Appl. Catal., A*, 1996, **137**, 25–36.
- 149 H. Lu, J. P. Kim, S. H. Son and J. H. Park, *Mater. Lett.*, 2011, **65**, 2858–2860.
- 150 J. Yi, M. Schroeder, T. Weirich and J. Mayer, *Chem. Mater.*, 2010, **22**, 6246–6253.
- 151 C. Galven, J.-L. Fourquet, E. Suard, M.-P. Crosnier-Lopez and F. Le Berre, *Dalton Trans.*, 2010, **39**, 4191–4197.
- 152 B. R. Sneha and V. Thangadurai, *J. Solid State Chem.*, 2007, **180**, 2661–2669.
- 153 F. Fujishiro, K. Fukasawa and T. Hashimoto, *J. Am. Ceram. Soc.*, 2011, **94**, 3675–3678.
- 154 J. Yi, T. E. Weirich and M. Schroeder, *J. Membr. Sci.*, 2013, **437**, 49–56.
- 155 M. T. Dunstan, W. Liu, A. F. Pavan, J. A. Kimpton, C. D. Ling, S. A. Scott, J. S. Dennis and C. P. Grey, *Chem. Mater.*, 2013, **25**, 4881–4891.
- 156 M. T. Dunstan, P. D. Southon, C. J. Kepert, J. Hester, J. A. Kimpton and C. D. Ling, *J. Solid State Chem.*, 2011, **184**, 2648–2654.
- 157 M. Li, K. Huang, J. A. Schott, Z. Wu and S. Dai, *Microporous Mesoporous Mater.*, 2017, **249**, 34–41.
- 158 Y. Zhou, K. Yan, Z. Yang, R. A. Bauer, N. Hong and H. Verweij, *ACS Appl. Nano. Mater.*, 2020, **3**, 6654–6663.
- 159 H. R. Amedi and M. Aghajani, *J. Nat. Gas Sci. Eng.*, 2016, **35**, 695–702.
- 160 N. Azizi, T. Mohammadi and R. M. Behbahani, *J. Energy Chem.*, 2017, **26**, 454–465.
- 161 W. Zhu, F. Liu, M. Gou, R. Guo and X. Li, *Green Chem. Eng.*, 2021, **2**, 132–143.
- 162 W. M. Aframehr, B. Molki, R. Bagheri, P. Heidarian and S. M. Davodi, *Chem. Eng. Res. Des.*, 2020, **153**, 789–805.
- 163 C. Cazorla, S. A. Shevlin and Z. X. Guo, *J. Phys. Chem. C*, 2011, **115**, 10990–10995.
- 164 J. Yu, L.-H. Xie, J.-R. Li, Y. Ma, J. M. Seminario and P. B. Balbuena, *Chem. Rev.*, 2017, **117**, 9674–9754.
- 165 B. Vujic and A. P. Lyubartsev, *Chem. Eng. Sci.*, 2017, **174**, 174–188.
- 166 X. Huang, J. Lu, W. Wang, X. Wei and J. Ding, *Appl. Surf. Sci.*, 2016, **371**, 307–313.
- 167 G. Avci, I. Erucar and S. Keskin, *ACS Appl. Mater. Interfaces*, 2020, **12**, 41567–41579.
- 168 G. Avci, S. Velioglu and S. Keskin, *ACS Appl. Mater. Interfaces*, 2018, **10**, 33693–33706.
- 169 H. Fang, A. Kulkarni, P. Kamakoti, R. Awati, P. I. Ravikovitch and D. S. Sholl, *Chem. Mater.*, 2016, **28**, 3887–3896.
- 170 C. Shi, L. Li and Y. Li, *J. CO2 Util.*, 2020, **42**, 101346.

